5345

5343

A linear stability analysis of the spatially-developing incompressible plane laminar mixing layer using minimal composite theory

A Thesis

Submitted for the Degree of

MASTER OF SCIENCE (ENGINEERING)

by

PINAKI BHATTACHARYA

ENGINEERING MECHANICS UNIT
JAWAHARLAL NEHRU CENTRE FOR ADVANCED SCIENTIFIC
RESEARCH
(A Deemed University)
Bangalore – 560 064

AUGUST 2007

To myself, no less!

DECLARATION

I hereby declare that the matter embodied in the thesis entitled "**Linear stability analysis of the mixing-layer using minimal composite theory**" is the result of investigations carried out by me at the Engineering Mechanics Unit, Jawaharlal Nehru Centre for Advanced Scientific Research, Bangalore, India under the supervision of Prof. Roddam Narasimha and Prof. Rama Govindarajan and that it has not been submitted elsewhere for the award of any degree or diploma.

In keeping with the general practice in reporting scientific observations, due acknowledgment has been made whenever the work described is based on the findings of other investigators.
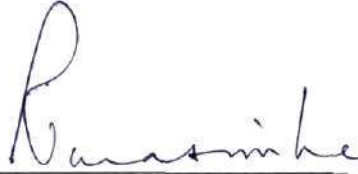
Pinaki Bhattacharya

CERTIFICATE

We hereby certify that the matter embodied in this thesis entitled "**Linear stability analysis of the mixing layer using minimal composite theory**" has been carried out by Mr. Pinaki Bhattacharya at the Engineering Mechanics Unit, Jawaharlal Nehru Centre for Advanced Scientific Research, Bangalore, India under our supervision and that it has not been submitted elsewhere for the award of any degree or diploma.

Prof. Roddam Narasimha
(Research Supervisor)

Prof. Rama Govindarajan
(Research Supervisor)

Acknowledgements

Summary

The aim of the present work is to undertake a non-parallel linear stability analysis of the two-dimensional incompressible mixing layer. The theory takes into account all the effects of streamwise variation upto $O\left(\text{Re}^{-1}\right)$. The Reynolds number Re is based on the vorticity-thickness δ_ω as the length scale and the velocity difference Δ between the free streams as the velocity scale. This follows from the minimal composite theory developed in Govindarajan & Narasimha (1995, 1997) and applied to the boundary layers in Govindarajan & Narasimha (2005), where it is shown to yield solutions accurate to $O\left(\text{Re}^{-1}\right)$ without having to solve the full non-parallel flow partial differential equation. The theory is employed here towards a spatial stability analysis of the similarity solution for the mixing layer obtained from lowest-order boundary-layer theory.

According to classical parallel stability analysis applied to the mixing layer (Betchov & Szewczyk, 1963; Esch, 1957) the critical Reynolds number is zero. This analysis follows from the well-known Orr–Sommerfeld equation which assumes that the mean flow is invariant in the streamwise direction x. The result from parallel theory holds for all disturbance quantities and along all trajectories in the flow-domain.

In the present work, the disturbance kinetic-energy integrated along the similarity coordinate y at a given streamwise location is representative of the level of perturbation in the mixing layer. The growth rate of this particular quantity is used to define the stability boundary of the mixing layer. It is found that the mixing layer is then stable for all $\text{Re} < \text{Re}_c \approx 30$, irrespective of the free stream velocity ratio (but not including cases with counterflow), and this is the main result of this thesis.

The present non-parallel analysis retains considerable mathematical tractability without making any of the customary simplifications - namely flow parallelism, inviscid dynamics of the perturbation field, temporal analysis, simple universal

velocity profile - that were necessary in all earlier work (Betchov & Szewczyk, 1963; Esch, 1957; Michalke, 1965). The assumptions made in the present analysis, however unrestrictive, are appraised in the light of the result quoted above, i. e. $Re_c \approx 30$. These assumptions follow from the requirement that the Reynolds number be sufficiently large. Using a well-known definition from measure theory, it is demonstrated that along the marginal stability boundary the analysis may be deemed satisfactory.

Publications

Refereed Paper

Bhattacharya, P., Manoharan, M. P., Govindarajan, R. & Narasimha, R. 2006 The critical Reynolds number of a laminar incompressible mixing layer from minimal composite theory. *J. Fluid Mech.* **565**, 105–114.

Conference Paper

Is a stable laminar mixing layer possible?, by Pinaki Bhattacharya, Rama Govindarajan and R. Narasimha, presented at the 11th Asian Congress of Fluid Mechanics held in Kuala Lumpur, Malaysia (May 2006).

Nomenclature

Roman Letters

A	:	Amplitude function
$\mathbf{A}, \mathbf{B}, \mathbf{F},$ $\mathbf{P}, \mathbf{L}, \mathbf{M}$	:	Coefficient matrices
c	:	Phase-speed of a particular normal-mode
$\mathbf{D}$	:	Derivative matrix for a Chebyshev cosine collocation-point distribution
f	:	Similarity streamfunction
$\mathcal{H}$	:	Higher-order operator
k	:	Disturbance kinetic-energy
$\mathcal{M}$	:	Minimal composite operator
$\mathcal{M}_\infty, \mathcal{M}_c$	:	Minimal operators in the far-field and the critical-layer respectively
$\mathcal{N}$	:	Non-parallel operator correct to $O\left(\mathrm{Re}^{-1}\right)$
$\mathcal{O}$	:	Orr–Sommerfeld operator
p	:	Non-dimensional constant, equals the ratio of the rate of change of vorticity-thickness in the streamwise direction with the inverse of the Reynolds number
$\bar{p}$	:	Mean flow pressure
$\hat{p}$	:	Amplitude of pressure perturbation of a particular normal-mode
Re	:	Reynolds number
$\mathcal{S}$	:	Streamwise-derivative operator
t	:	Time
U, V	:	Streamwise and normal velocity components of the mean flow respectively

$U_\infty, U_{-\infty}$:   Dimensional free stream velocity of the upper and lower streams respectively

u, v, w :   Perturbation velocity components of a particular normal-mode in the streamwise, normal and spanwise directions respectively

$\hat{u}, \hat{v}, \hat{w}$:   Amplitude of velocity perturbation components of a particular normal-mode, in the streamwise, normal and spanwise directions respectively

x :   Streamwise direction and coordinate

y :   Normal direction and coordinate; also similarity coordinate

z :   Spanwise direction and coordinate

Greek Letters

α :   Streamwise wavenumber of a particular normal-mode

β :   Spanwise wavenumber of a particular normal-mode

Δ :   Velocity-difference between the free streams

δ_c :   Characteristic thickness of the critical-layer

δ_ω :   Vorticity thickness

ϵ :   Magnitude of higher-order contribution, relative to lowest-order

Φ :   Mean flow streamfunction

ϕ :   Perturbation streamfunction of a particular normal-mode

$\hat{\phi}$:   Perturbation streamfunction amplitude

$\hat{\phi}_h$:   Higher-order streamfunction

$\hat{\phi}_m$:   Eigenfunction satisfying the minimal-composite operator

η :   Similarity coordinate

ν :   Kinematic vicosity of the fluid

Ω :   Perturbation vorticity of a particular normal-mode

ω :   Frequency identifying a particular normal-mode

Π :   Perturbation pressure of a particular normal-mode

ρ :   Density of the fluid

θ :   Characteristic thickness of the mixing layer

Subscripts

d   :   Dimensional quantity

i   :   Imaginary-part of a complex quantity

r   :   Real-part of a complex quantity

List of Figures

List of Tables

Contents

CHAPTER 1

INTRODUCTION

A laminar flow undergoing transition to turbulence passes through a succession of intermediate stages. The exercise of quantifying the onset of change from the initially laminar state is the realm of linear stability analysis. If the change from laminar state (mean flow) is precipitated by initially small disturbances (perturbations), then the immediate evolution of the perturbation is governed by the characteristics of the mean flow, but not vice-versa. That is to say there is no feedback mechanism, and hence a linear analysis is possible. Linear analysis is valid only as long as the amplitude of perturbation remains small compared to the mean flow. Any disturbance can then be decomposed into a sum of normal modes, as traveling waves for instance, identified by a wavenumber and a corresponding frequency.

Stability analysis can be classified as either temporal or spatial. In temporal analysis each mode either grows or decays in time, whereas in spatial analysis the modes grow or decay along the streamwise direction. The rate of growth (or of decay) characterizes the stability of the underlying mean flow. However we note that for the purpose of determining the curve of marginal stability, either analysis gives the same result.

Efforts at linear stability analysis of laminar flows can be classified according to their line of approach. Such branching out has happened primarily because different approaches present different mathematical challenges, and the advances

1

made in overcoming these challenges have been unequal. Understandably, some approaches have received much more attention compared to others.

For instance, inviscid dynamics for the perturbation field is easier to handle than the full viscous problem. This is because including the effects of viscous diffusion increases the order of the differential equation. The limitation of inviscid dynamics is that it can at best be representative of a high Reynolds number situation. If the onset of instability occurs at a low Reynolds number, then at sufficiently high Reynolds numbers the flow perhaps reaches fully turbulent state where the linear assumption is invalid. Moreover, the information conveyed by inviscid dynamics is not useful to predict the stability behaviour at low Reynolds numbers.

Similarly, since in spatial analysis the eigenvalue problem is non-linear in the wavenumber, there are limitations to the analytical tractability of the problem. Therefore much of the initial headway was made using the temporal approach. For example viscous temporal analysis of the mixing layer was carried out by Betchov & Szewczyk (1963). It was later shown by Michalke (1965), who did an inviscid spatial analysis of the mixing layer, that to make theory correspond with real flows spatial theory would be the more meaningful choice.

Linear stability analyses have therefore been combinations of choices from the several distinctions made above. Yet another ramification arises out of the specification of the mean flow. If the mean velocity flow profile can be expressed analytically, which is often only an approximation to the real flow, then the mathematical treatment proceeds along easier lines. The coefficients in the governing equations for the disturbance field are functions of the mean flow profile. Therefore an analytical specification of the mean flow profile enables mathematical simplifications like integration, order approximation, transformation of variables, etc. Examples pertaining to the mixing layer are Monkewitz & Huerre (1982) who present a spa-

tial inviscid analysis of a hyperbolic tangent profile, and Balsa (1987) who carries out a spatial viscous analysis of piecewise-linear profiles.

Another difference often made is whether the mean flow is to be considered non-parallel, that is developing in the streamwise direction, or not. If the mean flow is assumed to be parallel i.e. homogenous in the streamwise direction, the governing equations are ordinary differential equations. The Orr–Sommerfeld equation, due to Orr (1907) and Sommerfeld (1908), is an ordinary differential equation in the normal coordinate y, and has been widely used. On the other hand for a non-parallel problem, a set of partial differential equations has to be usually solved. Since the mathematical machinery for solving ordinary differential equations is well-developed, reduction to ordinary differential equations is a valuable simplification if an analytical treatment is desired. For solving partial differential equations, a computational procedure has to be resorted to, almost as a rule.

To our knowledge a non-parallel linear stability analysis of the mixing layer, that consistently accounts for all the effects of streamwise variation, has not been undertaken before. The only attempt at reconciling non-parallelism was made by Lessen & Ko (1966) and Ko & Lessen (1969), but we find their approach ad-hoc. For instance they neglected the effect on the non-parallel growth-rate due to the change in the shape of the disturbance streamfunction. In previous studies (see for e.g. Govindarajan & Narasimha, 1997, 2005) it was shown that the interplay between various agents contributing to the non-parallel growth-rate is subtle. In fact it is shown in the present work that, though the critical Reynolds number Lessen & Ko (1966) and Ko & Lessen (1969) report is of the same order as presented here, their analysis is contradictory to the one in this thesis.

The present situation is as follows. All previous analyses (Balsa, 1987; Betchov & Szewczyk, 1963; Esch, 1957; Huerre & Monkewitz, 1985; Ko & Lessen, 1969;

Lessen & Ko, 1966; Michalke, 1965) have led to insights into mixing layer insta-bility dynamics or to other analyses, but no single analysis includes both viscous effects and non-parallelism. For example neglecting viscosity from the perturbation dynamics cannot describe stability behaviour at low Reynolds number. As Huerre & Monkewitz (1985) showed, temporal stability results cannot be converted to spa-tial stability characteristics using the transformation due to Gaster (1962), which is not applicable to mixing layers with sufficiently strong counterflow. Though it has been noted that for open-shear flows like the mixing layer the dependence of the stability characteristics on the exact velocity profile is weak (Lin, 1955), results from analyses on hypothetical profiles like Esch (1957) lead to unnatural kinks in the marginal stability curve.

However the critical problem is that of considering the mean flow to be parallel. Neglecting the developing nature of the mean flow, even after including other diffi-cult aspects of analysis, still gives the critical Reynolds number to be zero (Betchov & Szewczyk, 1963; Drazin & Reid, 2004). Not only is this result unphysical in the face of energy theories (see below) but also the wavenumber going to zero as Re $\rightarrow$ 0 poses a serious doubt on the validity of the parallel analysis. Lessen & Ko (1966) noted that a relevant measure of flow non-parallelism is the change in the thickness of the mixing layer over one wavelength of the disturbance mode. Now a vanish-ing wavenumber implies an infinitely long wave. The change in the mixing layer thickness over one wavelength is therefore not negligible by any means.

If the problem includes mean flow non-parallelism, the coefficients of the per-turbation evolution operator are dependent on the streamwise coordinate and so-lutions in the form of constant speed traveling waves cannot be sought. Even if the variation in the streamwise direction is assumed to be small, and wave*like* solutions are sought, care must be taken to describe the mode because the dispersion rela-

tion connecting wavenumber and frequency varies along the streamwise direction. These present challenges in their own right and promise to make non-parallel linear stability analysis of the mixing layer rewarding.

A separate yet significant line of development pertaining to spatially developing flows is that of global stability (Chomaz, 2005; Huerre & Monkewitz, 1990) which can be employed in the case of strongly non-parallel flows as well. But these studies concern themselves primarily with the $Re = \infty$ limit. Moreover, it is the temporal growth rate of perturbations that is investigated in these analyses. Thus the question of spatial stability at low Reynolds number remains unanswered.

The paramount motivating factor for undertaking a non-parallel analysis, however, especially in the case of the mixing layer, arises out of energy theories (Joseph, 1966; Lin, 1955; Lorentz, 1907) that insist that there must exist a finite Reynolds number, however small, below which viscosity must damp out all tendency for disturbance growth. Since viscosity is the agent that contributes to flow non-parallelism, it is expected that non-parallelism cannot be neglected at low Reynolds numbers (Bun & Criminale, 1994; Drazin & Reid, 2004). In fact, flow non-parallelism is unbounded at $Re = 0$, and must therefore be included to understand the dynamics at low Reynolds numbers.

The mixing layer is a prototypical flow that is contained in other more complex flows. For example, velocity profiles display inflexion points in the flow over a rotating annulus (Solomon et al., 1993), a rotating disk (Lingwood, 1995), in a jet issuing into a crossflow (Yuan et al., 1999), in coaxial jets (Villermaux & Rehab, 2000), during spray formation (Marmottant & Villermaux, 2004), in a boundary-layer over a swept-wing (Craik, 1980), in the initial shedding region behind a stationary cylinder in a uniform flow (Stegner et al., 2005), etc. Results from mixing layer instability analysis have been applied to these problems, and in turn these studies

have contributed significantly to the literature on mixing layer dynamics.

This thesis is structured as follows. In chapter 2 the derivation of the similarity solution is outlined. Suitable non-dimensionalization is introduced that will subsequently be used everywhere. In chapters 3 and 4 the existing parallel flow theory is revisited and the results are presented as a validation of the numerical procedure used in the sequel. In chapter 5 the minimal composite theory, as applied to the mixing layer, is considered in detail, with the analysis following in chapter 6. To conclude the results are presented in chapter 7 with a remark on the substantial improvement obtained over parallel analysis.

Jon Arbuckle: You didn't follow that! How come?
Garfield: Because I am a cat.
- some creatures overheard discussing the present chapter.

CHAPTER 2

LAMINAR MIXING LAYER: SIMILARITY

SOLUTION

The linear stability analysis of a given laminar flow, henceforth called the mean flow, is concerned with determining whether it is stable or unstable to infinitesimally small perturbations. Therefore describing the mean flow is the first step of the problem.

Note that since the perturbations are infinitesimally small, they do not affect the evolution of the mean flow. Therefore, in principle, the perturbation field and the mean flow may be governed by different dynamics. For example, the mean flow may be inviscid while the perturbation-field has to include viscosity effects, and vice versa. Hypothetical mean flow profiles that have been used in the context of the mixing layer in linear stability literature include the piecewise linear, tanh, error-function, etc., a compilation of which appears in Esch (1957).

This chapter presents the mean flow for the two-dimensional incompressible mixing layer. The description follows from the boundary-layer approximation, which is an asymptotically valid description of the real flow for sufficiently large Reynolds numbers. Restrictions on the approximation are discussed later in this chapter.

7
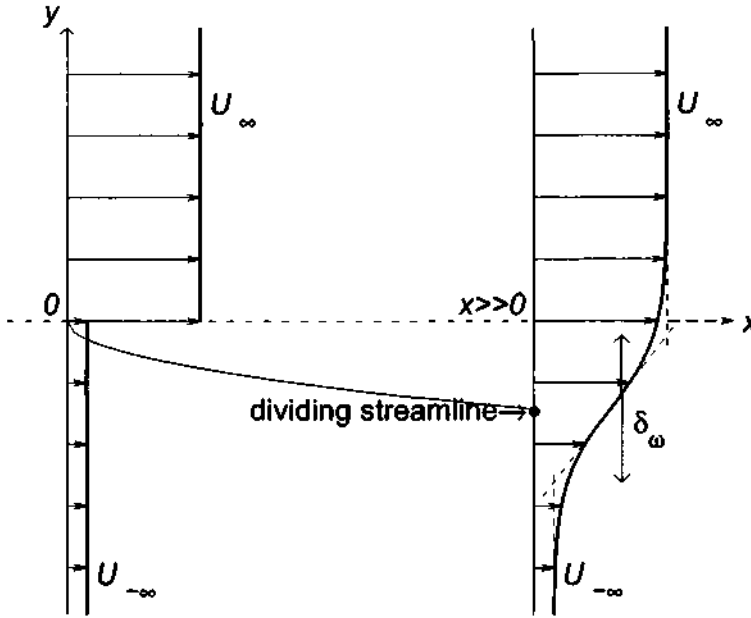
Figure 2.1: Schematic of the plane mixing layer.

2.1   The two-dimensional incompressible mixing layer

Figure 2.1 shows the two-dimensional incompressible mixing layer. Two uniform streams flow at velocities U_∞ and $U_{-\infty}$. The sign of U_∞ and $U_{-\infty}$ is taken to be the same, that is the streams flow in the same direction. This common direction of flow is called the streamwise direction and is denoted by the axis x_d. If U_∞ and $U_{-\infty}$ are opposite in sign, the case is called a mixing layer with backflow. It is outside the scope of the present study because the streamwise direction is then ill-defined and so is the non-parallelism which is the thrust of this work.

The two free streams occupy the regions $(-\infty, 0]$ and $[0, \infty)$ in the direction normal to the streamwise - denoted by axis y_d - before merging at $x_d = 0$. The velocity difference between the streams, $\Delta = (U_\infty - U_{-\infty})$, manifests as a source of vorticity that diffuses into the free streams as the flow advances in the streamwise

direction. Due to the diffusion process the region of mixing grows wider with x_d, while the velocity difference Δ remains a constant. A velocity-ratio parameter Λ based on Δ is defined as

$$\Lambda \equiv \frac{(U_\infty - U_{-\infty})}{(U_\infty + U_{-\infty})} = \frac{(\Delta/U_\infty)}{2 - (\Delta/U_\infty)}. \tag{2.1}$$

Values of Λ equal to $1, 3/5, 1/3, 1/7$ and $1/39$ correspond to the ratio of the slower to the faster free stream $(U_{-\infty}/U_\infty)$ being 0, 0.25, 0.5, 0.75 and 0.95 respectively. For $0 \leq U_\infty \leq U_{-\infty}$ we have $1 \geq \Lambda \geq 0$.

The mean flow is assumed to be steady and two-dimensional. The equations governing the mean flow are thus the continuity equation and momentum equations in the x_d and y_d directions,

$$\frac{\partial U_d}{\partial x_d} + \frac{\partial V_d}{\partial y_d} = 0, \tag{2.2}$$

$$U_d \frac{\partial U_d}{\partial x_d} + V_d \frac{\partial U_d}{\partial y_d} = -\frac{1}{\rho} \frac{\partial \bar{p}_d}{\partial x_d} + \nu \left(\frac{\partial^2 U_d}{\partial x_d^2} + \frac{\partial^2 U_d}{\partial y_d^2} \right) \tag{2.3}$$

$$\text{and} \quad U_d \frac{\partial V_d}{\partial x_d} + V_d \frac{\partial V_d}{\partial y_d} = -\frac{1}{\rho} \frac{\partial \bar{p}_d}{\partial y_d} + \nu \left(\frac{\partial^2 V_d}{\partial x_d^2} + \frac{\partial^2 V_d}{\partial y_d^2} \right), \tag{2.4}$$

where U_d and V_d are the dimensional velocities in the streamwise and normal directions respectively, the spanwise velocity $W_d = 0$ everywhere, $\bar{p}_d$ is the pressure and ν and ρ are the (constant) kinematic viscosity and density of the fluid respectively. To provide a complete description of the flow equations (2.2)–(2.4) must be solved for the three unknowns U_d, V_d and $\bar{p}_d$, after being augmented by suitable boundary conditions.

2.2 Boundary-layer approximation

It was remarked earlier that the diffusion due to viscosity causes the mixing layer width to grow in the streamwise direction. To quantify this width, $\theta(x_d)$, we first assume that flow quantities change appreciably in the normal direction over a distance of order θ, while a change of similar order occurs over a distance x_d in the streamwise direction. (Note that θ is x_d dependent which takes into account the developing nature of the mixing layer.) Then we make the boundary-layer assumption $\theta \ll x_d$, which implies $\partial/\partial y_d \gg \partial/\partial x_d$. Therefore the rate of change is an order of magnitude higher in the normal direction compared to that in the streamwise. A typical boundary-layer analysis of (2.2)–(2.4) (Schlichting & Gersten, 2004, pp. 175–176) gives at the lowest-order

$$\frac{\partial U_d}{\partial x_d} + \frac{\partial V_d}{\partial y_d} = 0, \tag{2.5}$$

$$\text{and} \quad U_d\frac{\partial U_d}{\partial x_d} + V_d\frac{\partial U_d}{\partial y_d} = \nu\frac{\partial^2 U_d}{\partial y_d^2}. \tag{2.6}$$

Equations (2.5)–(2.6) are sufficient to solve for the two unknowns U_d and V_d, since the pressure-gradient term, being of higher order, drops out. Further, these equations admit a similarity transformation

$$U_d = f'(\eta)U_\infty, \tag{2.7}$$

where

$$\eta \equiv \frac{y_d}{\theta} \quad \text{and} \quad \theta = \sqrt{\frac{\nu x_d}{U_\infty}}. \tag{2.8}$$

Here η and f are the similarity coordinate and streamfunction respectively. Note that θ and U_∞ are, respectively, the length and velocity scales. Thus it follows

from the boundary-layer assumption that the mixing layer width $\theta \propto x_d^{1/2}$. We will take the dividing streamline, given by $f = 0$, to be located at $\eta = \eta_0$. The stream-function f satisfies the continuity equation (2.5) by definition, and the streamwise momentum equation (2.6) becomes

$$\frac{1}{2}ff'' + f''' = 0, \qquad (2.9)$$

which is called the similarity equation, first obtained and solved by Lock (1951). The streamwise velocity profile has an inflexion point where $f''' = 0$, say at $\eta = \eta_s$. From (2.9) the dividing streamline η_0 is seen to be identical to the inflexion point η_s, since the slope of the streamwise velocity f'' is zero only far away from the core of the mixing region.

2.3 Boundary conditions

The third-order ordinary differential equation (2.9) needs to be augmented with three boundary conditions. Two of these are straightforward and follow from the fact that the streamwise velocities must attain free stream speeds at distances far away from the mixing region:

$$f'(\infty) = 1 \quad \text{and} \quad f'(-\infty) = \frac{1-\Lambda}{1+\Lambda}. \qquad (2.10)$$

The third boundary condition is however not intuitive, indeed it has been the topic of much debate. This condition has sometimes (Schlichting & Gersten, 2004; Ting, 1959; von Karman, 1921) been specified as

$$\left.(\eta f' - f)\right|_{\infty} + \left(\frac{1-\Lambda}{1+\Lambda}\right)\left.(\eta f' - f)\right|_{-\infty} = 0, \qquad (2.11)$$

known as the von Karman zero net-transverse flux condition, and is probably the most prevalent in literature. Different conditions that other workers have used appear in Kundu & Cohen (2005, p. 373).

The boundary-value problem above was posed in yet another way by Monkewitz & Huerre (1982). They translated the similarity coordinate η to $\xi = \eta - \eta_s$, such that in the new coordinates $\xi = 0$ corresponds to the inflexion point η_s above. The similarity equation can be solved separately for $\xi \in (-\infty, 0]$ and $\xi \in [0, \infty)$ as initial-value problems by setting $f(0) = f'''(0) = 0$ and the slope of the streamwise velocity at the inflexion point $f''(0)$ imposed externally. With these initial conditions, the free stream velocities are obtained by integrating through $\xi \in [0, \pm\infty)$. In practice, the integral is carried out till the slope of the streamwise velocity f'' becomes sufficiently small. The upper and lower free stream velocities thus obtained determine the solution f for a particular Λ which is obtained a posteriori. Thus there is a one-to-one correspondence between $f''(0)$ and Λ. In this method, the non-intuitive von Karman boundary condition above is not required but the location of the inflexion point is left unspecified. Though either specification gives the same result, equation (2.11) was used in the present calculation.

2.4   Numerical solution

The boundary-value problem (2.9)–(2.11) is solved using the *bvp4c* routine from the **MATLAB 6.0** suite. Equation (2.9) is cast in a first-order form

$$\frac{\mathrm{d}}{\mathrm{d}\eta} \begin{pmatrix} f_0 \\ f_1 \\ f_2 \end{pmatrix} = \begin{pmatrix} f_1 \\ f_2 \\ -\frac{1}{2} f_0 f_2 \end{pmatrix}, \qquad (2.12)$$

where $f_0 = f, f_1 = f'$ and $f_2 = f''$. Absolute tolerance is required to be $< 10^{-6}$. Relative value of tolerance was varied, but never exceeded 10^{-3} in magnitude.

Note that the boundary conditions need to be set at $\eta = \pm\infty$. For the computation, we substitute the infinite domain by a sufficiently large domain $\eta \in [-H, H]$ $(H > 0)$ and set the boundary conditions at $\eta = \pm H$ instead. The domain size is deemed to be sufficiently large when a further increase in its size does not change results by more than the tolerance specified. The finite domain is segregated into three parts each with a uniform spread of a sufficiently large number of grid points. Again, the number of grid points M is deemed sufficiently large when a further increase in its number does not change results by more than the specified tolerance. The three parts are such that the most dense clustering of points is around the location where the inflexion point is expected. This region is termed the core region. The least dense clustering of points is in the region of the domain farthest from the core region and is called the far-region. The intermediate region, called the outer-region, has a medium clustering density. A typical set of parameters used for different values of Λ is given in table 2.1.

2.5   Results

The vorticity-thickness

$$\delta_\omega \equiv \frac{|U_\infty - U_{-\infty}|}{\max |\partial U_d / \partial y_d|} = \theta \frac{|2\Lambda/(1 + \Lambda)|}{\max |f''|}, \tag{2.13}$$

can be defined once the similarity solution f is known. The ratio δ_ω/θ varies with Λ and appears in table 2.2 along with the location of the dividing streamline. Now

Run	Λ	δ_F	δ_O	δ_C	H_{fo}	H_{oc}	Rel. Tol.	η_s	δ_ω/θ	Residue
1	1	0.1	0.01	4×10^{-4}	25	1	1×10^{-4}	−0.5287	5.0083	8.77×10^{-4}
2	1	0.1	0.01	1×10^{-4}	25	1	1×10^{-4}	−0.5288	5.0083	8.77×10^{-4}
3	1	0.1	0.01	1×10^{-4}	25	1	1×10^{-3}	−0.5288	5.0083	1.13×10^{-3}
4	1	0.1	0.01	5×10^{-4}	25	3	1×10^{-3}	−0.5290	5.0083	1.13×10^{-3}
5	1	0.1	0.01	5×10^{-4}	25	3	1×10^{-4}	−0.5290	5.0083	8.77×10^{-4}
6	1	0.1	0.01	5×10^{-4}	25	3	1×10^{-4}	−0.5290	5.0083	8.77×10^{-4}
7	1	0.1	0.01	5×10^{-4}	25	3	1×10^{-4}	−0.5290	5.0083	8.77×10^{-4}
8	1	0.1	0.01	5×10^{-4}	25	3	1×10^{-4}	−0.5290	5.0083	8.77×10^{-4}
9	3/4	0.1	0.01	4×10^{-4}	25	1	1×10^{-4}	−0.5828	4.6821	-
10	3/5	0.1	0.01	4×10^{-4}	20	1	1×10^{-4}	−0.5548	4.4785	-
11	1/3	0.1	0.01	4×10^{-4}	20	1	1×10^{-4}	−0.3764	4.0915	-
12	1/7	0.1	0.01	4×10^{-4}	15	1	1×10^{-4}	−0.1676	3.7893	-
13	1/39	0.1	0.01	4×10^{-4}	10	1	1×10^{-4}	−0.0292	3.5901	-
14	1/7	0.1	0.01	4×10^{-4}	15	3	1×10^{-4}	−0.1676	3.7893	-

Table 2.1: Dependence of results on parameters of the computation. The spacing between adjacent grid-points in the far, outer and core regions is denoted by δ_F, δ_O and δ_C respectively. The boundary between the far and outer regions is at $\pm H_{fo}$, and that between the outer and core regions at $\pm H_{oc}$. Rel. Tol. is the relative tolerance value set before calling $bvp4c$ and the residue of the computation appears in the rightmost column. The point of inflexion (coinciding with the dividing streamline) is located at $\eta = \eta_s$ and δ_ω/θ is the non-dimensional vorticity-thickness.

Λ	0	1/39	1/7	1/3	3/5	3/4	1
δ_ω/θ	3.540	3.590	3.789	4.091	4.479	4.682	5.008
η_s	0	-0.029	-0.168	-0.377	-0.555	-0.583	-0.529

Table 2.2: Variation of the non-dimensionalized vorticity-thickness with velocity ratio.
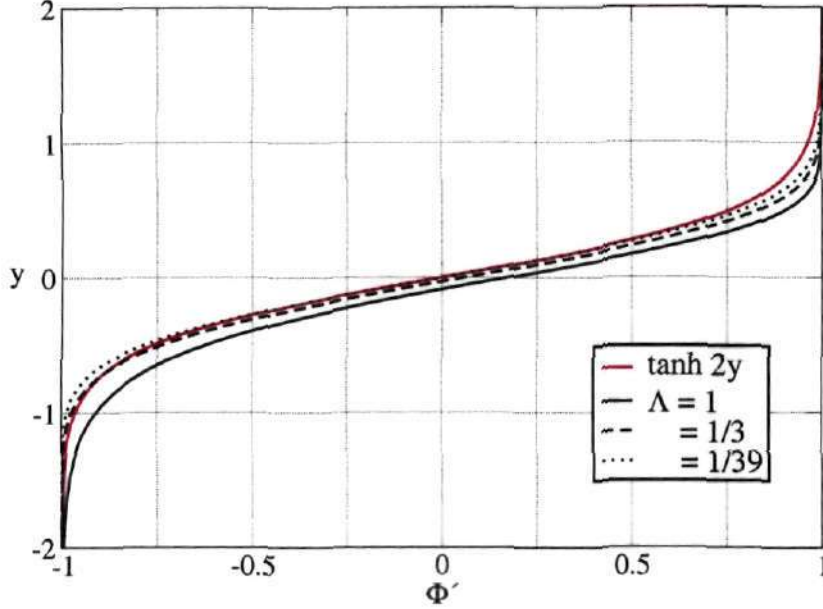
Figure 2.2: $\Phi'(y)$ obtained from the similarity solution for $\Lambda = 1$ (half-jet), 1/3 and 1/39 (nearly shear-less flow), compared with the $\tanh 2y$ profile.

the similarity coordinate and streamwise velocity are redefined as

$$y \equiv (\eta - \eta_s)\frac{\theta}{\delta_\omega}, \tag{2.14}$$

and

$$U_d = \left[\frac{1}{\Lambda} + \Phi'(y)\right]\frac{\Delta}{2}. \tag{2.15}$$

Note that $\Phi'(y = \pm\infty) = \pm 1$ for all Λ. The hyperbolic-tangent function $\tanh 2y$ bears a resemblance to $\Phi'(y)$ and figure 2.2 presents these functions for the cases $\Lambda = 1$, 1/3 and 1/39. For benchmarking purposes, we compare the location of the

dividing streamline η_s for the half-jet case ($\Lambda = 1$) from our computations with that from Schlichting & Gersten (2004, pp. 175–176). Note that in that analysis, the length-scale θ differs from the one in (2.8) by a constant multiple of $\sqrt{2}$. After accounting for this, the error between the two results is $|0.374\sqrt{2} - 0.529|/0.529 = 0.0001$, the match being excellent. Following Monkewitz & Huerre (1982), the Reynolds number is based on δ_ω and Δ as length and velocity scales respectively,

$$\mathrm{Re} \equiv \frac{\delta_\omega \Delta}{\nu}. \tag{2.16}$$

2.6   Comments

To obtain the value of δ_ω/θ for the limiting case of shear-less flow ($\Lambda = 0$), consider the generalized form of the similarity equation (2.9),

$$C f f'' + f''' = 0, \tag{2.17}$$

where $C = U_\infty \theta^2/2\nu x_d$ is an arbitrary constant, and the boundary-conditions (2.10)–(2.11) apply. (Here by leaving C unspecified, the particular definition of θ as in (2.8) has not yet been imposed.) Now assume the solutions to (2.17) corresponding to the two distinct boundary-conditions specified by Λ and $-\Lambda$ (in (2.10) and (2.11)) as f_1 and f_2 respectively. Further, suppose that the length-scale for f_2 is some $\tilde{\theta}$, different from θ used in the case of f_1. Applying the following two successive transformations

$$g(\zeta) \equiv -\left(\frac{1-\Lambda}{1+\Lambda}\right) f_2(\eta), \tag{2.18a}$$

$$\text{and} \quad \zeta \equiv -\eta, \tag{2.18b}$$

we have

$$\frac{dg}{d\zeta} = \dot{g} = \left(\frac{1-\Lambda}{1+\Lambda}\right) f_2'. \tag{2.19}$$

Similarly,

$$\ddot{g} = -\left(\frac{1-\Lambda}{1+\Lambda}\right) f_2'' \quad \text{and} \quad \dddot{g} = \left(\frac{1-\Lambda}{1+\Lambda}\right) f_2'''. \tag{2.20}$$

For $\tilde{\theta}$ and f_2, substituting the above transformation in (2.17), it follows that g satisfies

$$\left(\frac{U_\infty \tilde{\theta}^2}{2\nu x_d}\right) \left(\frac{1+\Lambda}{1-\Lambda}\right) g\ddot{g} + \dddot{g} = 0, \tag{2.21}$$

which implies that $g = f_1$ if

$$\frac{\tilde{\theta}}{\theta} = \sqrt{\frac{1-\Lambda}{1+\Lambda}} \tag{2.22}$$

and both g and f_1 satisfy the same boundary conditions. Now using the boundary conditions for f_2, equations (2.18) give

$$\dot{g}(\infty) = \left(\frac{1-\Lambda}{1+\Lambda}\right) f_2'(-\infty) = 1, \tag{2.23}$$

$$\dot{g}(-\infty) = \left(\frac{1-\Lambda}{1+\Lambda}\right) f_2'(\infty) = \left(\frac{1-\Lambda}{1+\Lambda}\right), \tag{2.24}$$

$$\text{and} \quad \dot{g}(\zeta\dot{g} - g)|_\infty + \dot{g}(\zeta\dot{g} - g)|_{-\infty} = 0, \tag{2.25}$$

which are identical to those for f_1.

Therefore the solution $g(\zeta)$ is exactly identical to $f(\eta)$. Now since

$$\frac{\delta_\omega(\Lambda)}{\theta} = \frac{|2\Lambda/(1+\Lambda)|}{\max|f_1''|} \quad \text{and} \quad \frac{\delta_\omega(-\Lambda)}{\tilde{\theta}} = \frac{|2\Lambda/(1-\Lambda)|}{\max|f_2''|}, \tag{2.26}$$

we have

$$\frac{\delta_\omega(\Lambda)}{\theta} = \frac{\delta_\omega(-\Lambda)}{\theta} \sqrt{\frac{1-\Lambda}{1+\Lambda}}. \tag{2.27}$$

From figure (2.3) we see that, in geometric configuration, f_1 and f_2 are essentially
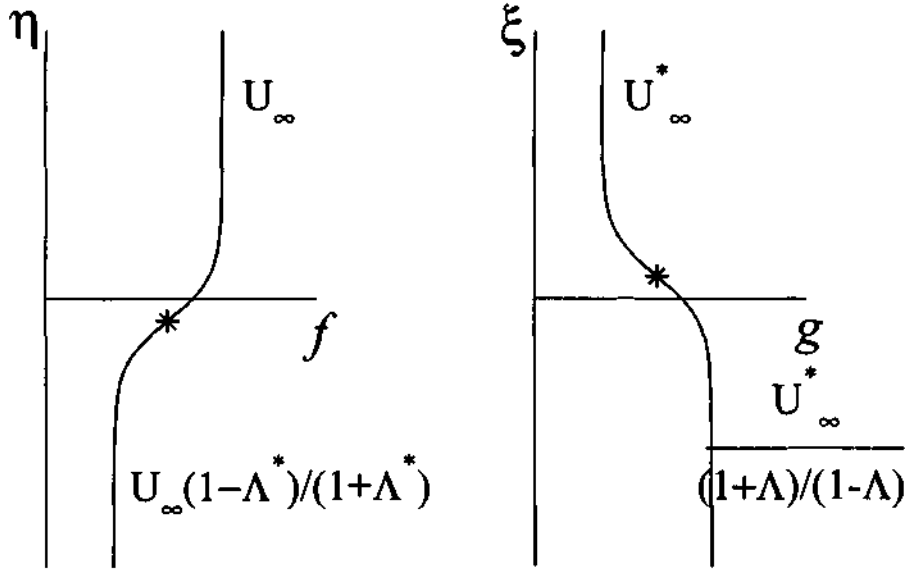
Figure 2.3: The original problem and its vertically-flipped counterpart.

vertically-flipped counterparts of each other.

Equation (2.27) can be used to obtain values of vorticity thickness for Λ equal to $-1/39$, $-1/7$, $-1/3$ etc. from those corresponding to $1/3$, $1/7$, $1/39$ (appearing in table 2.2). Using a smooth fit to these data through $\Lambda = 0$, we get the value of non-dimensional vorticity-thickness in the shear-less limit as 3.540. Monkewitz & Huerre (1982) used an asymptotic expansion, in powers of small Λ, of the similarity equation (2.9) to show that

$$\frac{\delta_\omega}{\theta}(\Lambda) = 2\sqrt{\pi} + O(\Lambda),$$

$$\Rightarrow \frac{\delta_\omega}{\theta}(\Lambda = 0) = 3.545,$$

which agrees well with our result.

CHAPTER 3

ORR–SOMMERFELD (PARALLEL) THEORY

Parallel-flow theory is concerned with the stability of a particular class of mean flows. The mean flow should be such that the only non-zero component of velocity is the streamwise velocity. From continuity it then follows that the streamwise velocity component is constant along streamlines. The gradient of the streamwise velocity in the direction normal to the flow, that is the shear, is the sole agent responsible for sustaining or inhibiting the growth of infinitesimally small perturbations. Mathematically, the mean flow can be expressed as $[U_d(y_d), 0, 0]$ where U_d is the dimensional velocity in the streamwise direction.

Parallel-flow theory is valid for strictly parallel flows like fully-developed flow in a pipe or channel. But due to the immense mathematical simplification it affords, this theory has also been applied to study the stability characteristics of flows that are not parallel, like open shear flows viz. the boundary-layer, jet, wake, mixing layer, etc. In this chapter, the Orr–Sommerfeld equation, which follows from the parallel-flow assumption, is derived. Subsequently, the method of determining the mixing layer stability characteristics from this equation is presented.

19

3.1   Limitations

For flows that are not parallel, employing parallel-flow theory necessitates the following approximations (Drazin & Reid, 2004, p. 154) in the mean flow

$$U_d \gg V_d \approx 0 \quad \text{and} \quad \frac{\partial U_d}{\partial y_d} \gg \frac{\partial U_d}{\partial x_d} \approx 0. \tag{3.1}$$

The theory therefore cannot be expected to describe the stability characteristics more faithfully than the approximation describes the reality for the mean flow. In other words, parallel theory has a good chance of being effective when applied to flows that are only slightly non-parallel. A measure of non-parallelism is the streamwise rate of growth of a characteristic length in the normal direction. If the local vorticity-thickness is taken to be such a characteristic length, then we require that δ_ω not change appreciably along the streamwise direction. From boundary-layer theory (see equations (2.1), (2.8), (2.13) and (2.16)) it follows that the rate of growth of the vorticity-thickness in the streamwise direction depends inversely on the local Reynolds number, and is given by

$$\frac{\mathrm{d}\delta_\omega}{\mathrm{d}x_d} = \left(\frac{\Lambda}{1+\Lambda} \right) \left(\frac{|2\Lambda/(1+\Lambda)|}{\max|f''|} \right)^2 \frac{1}{\mathrm{Re}} = \frac{p}{\mathrm{Re}}, \tag{3.2}$$

where p is a constant for a given Λ. (The variation of p with Λ is given in table 3.1.) Therefore at the origin, where the local Reynolds number is 0, the rate of growth of the vorticity-thickness is unbounded. Indeed, at $x_d \approx 0$, the boundary-layer assumption itself is suspect.

The Rayleigh equation omits the effect of viscosity altogether from the perturbation dynamics. The Orr–Sommerfeld equation would thus seem to improve upon the Rayleigh equation by including viscosity effects in the perturbation dy-

Λ	0	1/39	1/7	1/3	3/5	3/4	1
p	0	0.322	1.795	4.184	7.523	9.395	12.540

Table 3.1: Constant p, related to streamwise rate of growth of the vorticity-thickness, for different velocity ratios.

namics, thereby introducing the Reynolds number at a finite value. However, it has not been shown that the Orr–Sommerfeld equation is an asymptotically correct formulation at any finite Reynolds number, however, large, for a non-parallel flow.

Nevertheless, parallel-flow theory has attracted considerable and continued attention for almost a century. To a large extent it shows reasonable agreement with experimental results in fairly wide class of flows (Corcos & Lin, 1984; Corcos & Sherman, 1976, 1984; Grosch & Jackson, 1991; Jackson & Grosch, 1991), and this is one reason for the support it enjoys. Though ad-hoc and inconsistent in formulation for a non-parallel flow at any finite Re, the substantial literature in this field makes it a useful starting point, if not for developing non-parallel theory, then at least for comparing results.

3.2   Advantages

The principal advantage of assuming the mean flow to be invariant in the streamwise direction is that constant-speed traveling wave solutions are allowed. This follows from the fact that the coefficients in the operator governing the perturbation dynamics are then independent of x_d and a Fourier-transform is admissible.

The linearized equations for momentum and continuity of the perturbation field

$\{u_d, v_d, w_d, p_d\}$ on a parallel flow $(U_d, 0, 0)$ are

$$\frac{\partial u_d}{\partial x_d} + \frac{\partial v_d}{\partial y_d} + \frac{\partial w_d}{\partial z_d} = 0, \tag{3.3}$$

$$\frac{\partial u_d}{\partial t_d} + U_d \frac{\partial u_d}{\partial x_d} + v_d \frac{\partial U_d}{\partial y_d} = -\frac{1}{\rho}\frac{\partial \Pi_d}{\partial x_d} + \nu \nabla_d^2 u_d, \tag{3.4}$$

$$\frac{\partial v_d}{\partial t_d} + U_d \frac{\partial v_d}{\partial x_d} = -\frac{1}{\rho}\frac{\partial \Pi_d}{\partial y_d} + \nu \nabla_d^2 v_d \tag{3.5}$$

$$\text{and} \quad \frac{\partial w_d}{\partial t_d} + U_d \frac{\partial w_d}{\partial x_d} = -\frac{1}{\rho}\frac{\partial \Pi_d}{\partial z_d} + \nu \nabla_d^2 w_d, \tag{3.6}$$

where $\nabla_d^2 = \partial^2/\partial x_d^2 + \partial^2/\partial y_d^2 + \partial^2/\partial z_d^2$ and z is the spanwise coordinate. Following the method of normal modes, each perturbation quantity q_d is decomposed into a sum of traveling waves. Each wave is identified by a frequency ω_d and wavenumbers α_d and β_d in the streamwise and spanwise directions respectively. If $\hat{q}_d$ be the amplitude of each such wave, then it must depend only on y_d, since all coefficients of the perturbation quantities in equations (3.3)–(3.6) depend only on y_d. Moreover, due to the linearity property, the above equations can be written down separately for each mode. For the sake of brevity, we substitute for each q_d, the set $\{\hat{q}_d, \omega_d, \alpha_d, \beta_d\}$ corresponding to only one mode. The summation over all possible modes is implicit. The disturbance velocity and pressure fields are therefore

$$\{u_d, v_d, w_d\} = \Delta\{\hat{u}, \hat{v}, \hat{w}\} \exp\left[\mathrm{i}\left(\alpha_d x_d + \beta_d z_d - \omega_d t_d\right)\right], \tag{3.7}$$

$$\text{and} \quad \Pi_d = \frac{\rho \Delta^2}{2}\hat{p} \exp\left[\mathrm{i}\left(\alpha_d x_d + \beta_d z_d - \omega_d t_d\right)\right]. \tag{3.8}$$

Note that the velocities are non-dimensionalized by Δ whereas the pressure is non-dimensionalized by $(1/2)\rho\Delta^2$. The mean flow being two-dimensional, a theorem due to Squire (1933) is applicable (Drazin & Reid, 2004, p. 155) and hence only two-dimensional disturbances $(w_d = 0, \beta_d = 0, \partial/\partial z_d = 0)$ are considered. This

reduces (3.6) to an identity. Since the mean flow is parallel, the characteristic width of the mixing layer does not change with the streamwise direction. Therefore we assume an arbitrary but constant value for the vorticity-thickness and non-dimensionalize the rest of the quantities as follows:

$$
\left.
\begin{aligned}
\omega_d &= \omega\Delta/\delta_\omega, & t_d &= t\delta_\omega/\Delta, \\
x_d &= x\delta_\omega, & y_d &= y\delta_\omega \\
\text{and} \quad \alpha_d &= \alpha/\delta_\omega.
\end{aligned}
\right\}
\tag{3.9}
$$

Now, a perturbation streamfunction ϕ_d is defined as

$$
\phi_d = (\delta_\omega\Delta)\hat{\phi}(y)\exp\left[i\left(\alpha x - \omega t\right)\right],
\tag{3.10}
$$

such that

$$
u_d = \frac{\partial\phi_d}{\partial y_d} \quad \text{and} \quad v_d = -\frac{\partial\phi_d}{\partial x_d}.
\tag{3.11}
$$

The streamfunction in (3.10) automatically satisfies the perturbation continuity equation (3.3) and the amplitudes $\hat{u}$ and $\hat{v}$ are given by

$$
\hat{u} = D\hat{\phi} \quad \text{and} \quad \hat{v} = -i\alpha\hat{\phi},
\tag{3.12}
$$

where $D \equiv \partial/\partial y (= d/dy)$. Taking the curl of the perturbation velocity given by (3.4) and (3.5) to eliminate the pressure, and substituting (3.7), (3.9) and (3.12) in the resulting equation, we get

$$
\mathcal{O}\hat{\phi} = 0,
\tag{3.13}
$$

where

$$\mathcal{O} \equiv \left(\frac{1}{2\Lambda} + \frac{\Phi'}{2} - c\right)(D^2 - \alpha^2) - \frac{1}{2}\Phi''' - \frac{1}{i\alpha Re}(D^2 - \alpha^2)^2, \qquad (3.14)$$

which is the well-known Orr–Sommerfeld operator. Note that all x_d-derivatives of the mean flow have been dropped and the streamwise velocity is expressed as Φ'. Here $c = c_r + ic_i = \omega/\alpha$ is the non-dimensional complex phase-speed of the particular mode.

The other advantage of employing the Orr–Sommerfeld equation is realized in the following. Consider the term in (3.14) containing Re in the denominator, which is due to viscous diffusion. If this is dropped, we retrieve the Rayleigh equation

$$\mathcal{R}\,\hat{\phi} = 0, \qquad (3.15)$$
$$\text{where} \quad \mathcal{R} \equiv \left(\frac{1}{2\Lambda} + \frac{\Phi'}{2} - c\right)(D^2 - \alpha^2) - \frac{1}{2}\Phi''' \qquad (3.16)$$

is the inviscid Rayleigh operator. The first term in (3.16), proportional to the disturbance vorticity amplitude $(D^2 - \alpha^2)\hat{\phi}$ represents a competition between two agents: the temporal fluctuation of disturbance vorticity observed at a given location due to wave-motion and the advection of disturbance vorticity away from or into that location by the mean streamwise velocity. This balance is exact at the critical point y_c defined by $\Phi'(y_c) = 2c_r - (1/\Lambda)$.

Therefore at $y = y_c$ the Rayleigh equation is singular (Schmid & Henningson, 2001, p. 46). The viscous diffusion term in the Orr–Sommerfeld equation smooths out the singularity by providing a sufficiently high spatial gradient of the perturbation vorticity. At the critical point balance is achieved between viscous diffusion of disturbance vorticity and advection of the mean streamwise vorticity by the dis-

turbance normal velocity $(1/2)\Phi'''\hat{\phi}$. The viscous term is thus effective when the lowest-order terms cancel out.

Tollmien (1935) argued that for flows that are unbounded and two-dimensional the Orr–Sommerfeld operator has a neutrally stable mode, the wave-speed corresponding to which equals the mean streamwise velocity at the inflexion point. This result is applicable to the plane mixing layer with parallel-flow assumption, and implies $y_c = y_s$.

3.3 Eigenvalue problem

The eigenvalue problem (3.13) is a fourth-order differential equation and needs to be augmented by the four boundary conditions

$$D\hat{\phi} \to 0 \quad \text{and} \quad i\alpha\hat{\phi} \to 0, \qquad \text{as} \quad y \to \pm\infty, \qquad (3.17)$$

which require that both the disturbance velocity components vanish in the far-field. To set these conditions we rewrite (3.13) for $y \gg 1$, where $\Phi' \approx 1$ and $\Phi''' \approx 0$ (see figure 2.2). This gives

$$\left(\frac{1}{2\Lambda} + \frac{1}{2} - c\right)\left(D^2 - \alpha^2\right)\hat{\phi} - \frac{1}{i\alpha\mathrm{Re}}\left(D^2 - \alpha^2\right)^2\hat{\phi} = 0. \qquad (3.18)$$

The general solution to (3.18) that vanishes as $y \to \infty$ is given by

$$\hat{\phi} = C_{11}\,e^{-\alpha y} + C_{12}\,e^{-\gamma_1 y}, \qquad (3.19)$$

where

$$\gamma_1^2 = i\alpha\mathrm{Re}\left(\frac{1}{2\Lambda} + \frac{1}{2} - c\right) - \alpha^2 \qquad (\gamma_{1_r} > 0). \qquad (3.20)$$

Similarly the form of solutions at $y \ll -1$ is

$$\hat{\phi} = C_{21}\,e^{\alpha y} + C_{22}\,e^{\gamma_2 y}, \tag{3.21}$$

where

$$\gamma_2^2 = i\alpha\mathrm{Re}\left(\frac{1}{2\Lambda} - \frac{1}{2} - c\right) - \alpha^2 \qquad (\gamma_{2r} < 0). \tag{3.22}$$

Thus we expect exponentially decaying solutions. The boundary conditions are employed in two ways. The first choice is valid for large Re where the inviscid parts of the solution $C_{k1}e^{\pm\alpha y}$ ($k = 1, 2$) dominate. Hence the far-field solutions are assumed to satisfy

$$(\mathrm{D} \pm \alpha)\mathrm{D}\hat{\phi} = 0, \qquad \text{as} \quad |y| \gg 1. \tag{3.23}$$

Alternatively, we set the conditions,

$$\hat{\phi} = 0 \qquad \text{and} \qquad \mathrm{D}\hat{\phi} = 0, \qquad \text{as} \quad y \to \pm\infty, \tag{3.24}$$

where the domain is taken to be sufficiently large. The domain is deemed to be sufficiently large if a further increase in size does not change the solution by more than the computational accuracy.

3.4 Mode selection procedure

Note that (3.13) is a differential equation and therefore the operator $\mathcal{O}$ is infinite dimensional. Hence for a pair of (α, Re) an infinity of solutions ω is obtained. Similarly for a given (ω, Re) an infinite number of α are obtained. Gustavsson (1979) and Grosch & Salwen (1978) discuss in detail this continuous part of the spectrum.

For the problem of determining the stability boundary only of the most unstable mode need to be considered. However, since (3.13) and (3.17) will be solved numerically, only a finite number of modes is obtained depending on the number of points used to discretize the y-domain. Further, of these, some originate due to the numerical nature of the procedure. That is, these modes are unphysical and so must be rejected. Howard's semicircle theorem (Howard, 1961) restricts the phase-speed of physically valid growing modes of the inviscid Rayleigh operator to within a semicircular region of the complex c plane. The centre of the semicircle is at $(1/2\Lambda, 0)$ and its radius is $1/2$. This result, with some qualifications detailed below, is used to determine the most unstable mode in the spectrum.

First, we note that the Orr–Sommerfeld operator contains the Rayleigh operator as a subset. Further, the difference between the two operators scales as $\sim O\left(\mathrm{Re}^{-1}\right)$, and thus at high Re they become increasingly indistinguishable except at the critical layer and a wall layer when the mean flow is wall-bounded. It is therefore expected that the region of existence of physically valid phase-speeds of the Orr–Sommerfeld operator will also occupy a region not very different from Howard's semicircle. Secondly, from the argument due to Tollmien (1935) mentioned before, and from the fact that the difference between the velocity at the inflexion point and the average of the free stream velocities is much smaller than the radius of Howard's semicircle, that is $\Phi'(0)/2 \ll 1/2$, it is expected that a neutrally stable mode will lie closer to the centre of Howard's semicircle than to its periphery.

The mode selection is therefore as follows. A semicircular region centred at $(1/2\Lambda + \Phi'(0)/2, 0)$ in the complex c plane and with radius $b/2$ is searched. Here b is a positive fraction < 1. The most unstable eigenvalue in this region is denoted by $c \equiv c(\alpha, \omega, \mathrm{Re})$.

3.5   Growth rate

Consider a general perturbation quantity q of the form

$$q = \hat{q}(y) \exp\left[i\left(\alpha x - \omega t\right)\right]. \tag{3.25}$$

Note that the amplitude of the perturbation is only dependent on y following the parallel assumption. The temporal and spatial growth rates of q, respectively, are then given by

$$\left(\frac{1}{q}\frac{\partial q}{\partial t}\right)_r = \omega_i \qquad \text{and} \qquad \left(\frac{1}{q}\frac{\partial q}{\partial x}\right)_r = -\alpha_i. \tag{3.26}$$

where subscripts r and i denote the real and imaginary parts respectively.

CHAPTER 4

ORR–SOMMERFELD ANALYSIS AND RESULTS

In the present chapter the methodology of solving the Orr–Sommerfeld equation with the associated boundary conditions is detailed. The set of equations are cast into an eigenvalue problem. The choice of the eigenvalue is between the wavenumber and the frequency, depending on whether spatially or temporally growing waves are being sought. It was noted earlier that for the problem of computing the curve of marginal stability, both the choices give the same result. Therefore, both choices are considered in this chapter, the solution strategies are detailed separately and the results compared with those from reported studies. This exercise serves as a benchmark for the computational procedure used in the rest of this thesis.

Results from the analysis are also presented considering different prescriptions of the mean flow profile. Comparisons are made by suitably rescaling the profiles such that the broken-line profile, the hyperbolic tangent profile and the similarity profile have identical vorticity-thickness and dividing streamline location for a given Λ. It is well-known (following Drazin & Reid, 2004; Tatsumi & Gotoh, 1960; Tatsumi & Kakutani, 1958) that for free shear flows like the mixing layer stability characteristics depend chiefly on the integral quantities of the velocity profile and only weakly on its details. The results at the end of this chapter corroborate this conclusion.

4.1 Chebyshev collocation points

Consider the finite domain $y \in [-L, L]$. The coordinate-transformation

$$y = L \frac{\sinh S y_f}{\sinh S},$$ (4.1)

takes y to y_f, where S is a stretching factor that is controlled during the compu-
tation. The y_f-domain is between $[-1, 1]$, which is further discretized to a set of
Chebyshev cosine collocation points given by

$$y_{f_k} = \cos \frac{(k-1)\pi}{N-1}, \qquad k = 1, 2, \ldots, N$$ (4.2)

for odd values of N. Equation (4.1) ensures that equal spacing of y_{f_k} on the sinh-
grid corresponds in the physical domain to densely-packed points near the origin
and the ends, and sparsely distributed points elsewhere. It was noted earlier that
the perturbation field is expected to have high gradients near the critical point.
Also it is expected that the critical layer is close to the inflexion point $y = 0$
for marginally stable modes. Therefore the rapid change in the critical layer is
expected to be captured accurately using the grid-stretching (4.1). It also increases
the efficiency of the computation procedure for a given level of accuracy since a
smaller number of points suffice to cover the domain.

The mean flow profile details also need to be supplied at the same points where
the eigenfunction is evaluated. Recall from § 2.4 that the mean flow was computed
on a uniform-grid of finely-spaced points on the η-coordinate. The **MATLAB**
routine *bvpsol* is used to obtain the similarity solution on the sinh-grid.

4.2 Eigenvalue problem in ω

To formulate the temporal stability problem consider (3.13). The solution eigenfunction $\hat{\phi}$, written as a one-dimensional vector in $\mathbb{C}^N$,

$$\{\hat{\phi}\} \equiv [\hat{\phi}(y_1) \ \hat{\phi}(y_2) \ \ldots \ \hat{\phi}(y_N)]^{\mathrm{T}} \tag{4.3}$$

with $y_k = y(y_{f_k})$, satisfies

$$\mathbf{A}\{\hat{\phi}\} = \omega \, \mathbf{B}\{\hat{\phi}\}, \tag{4.4}$$

where ω is the complex frequency,

$$\begin{aligned}
\mathbf{A} &= (-1/i\mathrm{Re})(\mathbf{FD})^4 + (\alpha/2)\mathbf{P}_1(\mathbf{FD})^2 \\
&\quad + [(2\alpha^2/i\mathrm{Re}) + (\alpha/2\Lambda)](\mathbf{FD})^2 \\
&\quad - [(\alpha^3/2\Lambda) + (\alpha^4/i\mathrm{Re})]\mathbf{I} \\
&\quad - (\alpha^3/2)\mathbf{P}_1 - (\alpha/2)\mathbf{P}_3,
\end{aligned} \tag{4.5}$$

$$\mathbf{B} = (\mathbf{FD})^2 - (\alpha^2)\mathbf{I}, \tag{4.6}$$

$$(\mathbf{F})_{ij} = \begin{cases} 0 & \text{if } i \neq j, \\ \left(\dfrac{\sinh S}{LS}\right)\mathrm{sech} S y_{f_i} & \text{if } i = j \end{cases} \tag{4.7}$$

and

$$(\mathbf{P}_1)_{ij} = \begin{cases} 0 \\ \Phi'(y_i) \end{cases} \quad \text{and} \quad (\mathbf{P}_3)_{ij} = \begin{cases} 0 & \text{if } i \neq j, \\ \Phi'''(y_i) & \text{if } i = j \end{cases}. \tag{4.8}$$

Here $\mathbf{I}$ is the $N \times N$ identity matrix and the derivative matrix $\mathbf{D}$ is given in Appendix B. Boundary conditions (3.23) are set as follows. Consider the matrix

equations

$$(\mathbf{FD} + \alpha\mathbf{I})\{\hat{\phi}\} = \omega\,\mathbf{0}\{\hat{\phi}\} \tag{4.9}$$

$$(\mathbf{FD} - \alpha\mathbf{I})\{\hat{\phi}\} = \omega\,\mathbf{0}\{\hat{\phi}\} \tag{4.10}$$

$$\text{and} \quad \mathbf{FD}\{\hat{\phi}\} = \omega\,\mathbf{0}\{\hat{\phi}\}, \tag{4.11}$$

where $\mathbf{0}_{ij}(= 0\,\forall\,i,j)$ is the zero matrix. The first row of the matrices operating on $\{\hat{\phi}\}$ on either side of (4.9) are used to replace the corresponding row of the matrices on either side of (4.4). Similarly, the first row of the matrices operating on $\{\hat{\phi}\}$ on either side of (4.11) are used to replace the second row of the matrices on either side of (4.4). This sets the boundary conditions at $y = y_1 = L$.

For the boundary conditions at $y = y_N = -L$, similar replacement of the last two rows of the matrices operating on $\{\hat{\phi}\}$ on either side of (4.4) by the last rows each of (4.10) and (4.11) is carried out. This procedure described above follows Srinivasan $et\ al.$ (1994). Boundary conditions (3.24) are set in a similar fashion.

In § 2.5, it was noted that the hyperbolic tangent function $\tanh 2y$ describes the similarity profile $\Phi'(y)$ quite closely (see figure 2.2). Hence from Betchov & Szewczyk (1963) it follows that the unstable wavenumbers vary in the range $[0, 2]$. For a fixed real α in this range, we try two initial guesses of Re and note the value of $\omega_i = \omega_i(\alpha, \text{Re})$. Using these two solutions a Newton–Raphson procedure is conducted to determine the value of Re where ω_i is zero. The tolerance is set to 10^{-6}. For every subsequent value of α, the last two values of Re corresponding to the previous value of α are used as the initial two guess values of Re. It is expected that both these values will be very close to the curve of marginal stability since it is smooth in the (α, Re) plane. Indeed the number of iterations required for convergence is quite small $(\sim 3 - 4)$.

Recall that if the matrix size is $N \times N$, the number of eigenvalues ω computed for a given (α, Re) pair will also be N. To reject purely numerical (that is physically spurious) modes the Howard semicircle theorem is used. The most unstable mode out of the ones that meet this criterion is denoted by $\omega_i = \omega_i(\alpha, \mathrm{Re})$. Recall that since (3.13) is linear in $\hat{\phi}$, any complex multiple of $\hat{\phi}$ is also an eigensolution. To present results and compare eigenfunctions, we use the following normalization condition

$$\max \left| \hat{\phi}(y) \right| = 1, \tag{4.12}$$

unless otherwise specified.

4.3 Eigenvalue problem in α

Following the companion-matrix method of Bridges & Morris (1984), the spatial problem is formulated by introducing the variables

$$\phi_0 = \{\hat{\phi}\}, \quad \phi_1 = \alpha\{\hat{\phi}\}, \quad \phi_2 = \alpha^2\{\hat{\phi}\} \quad \text{and} \quad \phi_3 = \alpha^3\{\hat{\phi}\}. \tag{4.13}$$

Using these, equation (3.13) can be recast into a set of equations with eigenvalue α appearing only in the first degree as follows,

$$\mathbf{L}_A \varphi = \alpha \mathbf{L}_B \varphi, \tag{4.14}$$

where

$$\mathbf{L}_A \equiv \begin{bmatrix} 0 & \mathbf{I} & 0 & 0 \\ 0 & 0 & \mathbf{I} & 0 \\ 0 & 0 & 0 & \mathbf{I} \\ \mathbf{L}_0 & \mathbf{L}_1 & \mathbf{L}_2 & \mathbf{L}_3 \end{bmatrix}, \tag{4.15}$$

$$\mathbf{L}_0 = (-\mathrm{i}\mathrm{Re}\omega)(\mathbf{FD})^2 - (\mathbf{FD})^4, \tag{4.16}$$

$$\mathbf{L}_1 = (-\mathrm{i}\mathrm{Re}/2)\mathbf{P}_3 + (\mathrm{i}\mathrm{Re}/2\Lambda)(\mathbf{FD})^2$$
$$+ (\mathrm{i}\mathrm{Re}/2)\mathbf{P}_1(\mathbf{FD})^2, \tag{4.17}$$

$$\mathbf{L}_2 = 2(\mathbf{FD})^2 + (\mathrm{i}\mathrm{Re}\omega)\mathbf{I}, \tag{4.18}$$

$$\mathbf{L}_3 = (-\mathrm{i}\mathrm{Re}/2\Lambda)\mathbf{I} - (\mathrm{i}\mathrm{Re}/2)\mathbf{P}_1, \tag{4.19}$$

$\varphi = [\phi_0 \ \phi_1 \ \phi_2 \ \phi_3]^{\mathrm{T}}$ and $\mathbf{L}_B$ is the $4N \times 4N$ identity matrix. Now the augmented problem (4.14) is solved for the variable φ. The boundary conditions for φ are

$$\varphi = 0, \ \mathrm{D}\varphi = 0 \qquad \text{at} \quad y = \pm L, \tag{4.20}$$

and are set in a manner similar to that detailed in the preceding section. The grid-stretching and collocation-point strategy are identical to those in the temporal problem. For a given value of pure real ω, two guesses of Re are used to get two corresponding values of the fully-complex eigenvalue α. Using the Newton–Raphson procedure described in the foregoing section, we arrive at the curve of marginal stability $\alpha_i(\omega, \mathrm{Re}) = 0$. The mode selection procedure and normalization are retained from the previous analysis.

Numerical zero is always set to smaller than 5×10^{-5}, whereas numerical infinity is taken as 10^6. The *ZGGEV* routine from **LAPACK** suite is used to solve the

matrix eigenvalue problems (4.4) and (4.14). To increase the efficiency of the algorithm, the diagonal (two-dimensional) matrices $\mathbf{F}$, $\mathbf{P}_1$, $\mathbf{P}_3$ and $\mathbf{L}_3$ are stored as (one-dimensional) vectors. These tolerance values are sufficient to ensure that the results reported herein are independent of them.

4.4 Results

In this section the results from the temporal stability computations are first presented. It is noted that through a Galilean-transformation the temporal problem for the tanh (or for any invariant) profile can be posed identically for different velocity ratios. Therefore we compare our computation on the tanh-profile for different ratios with those in Betchov & Szewczyk (1963). Following this, comparison is made between the computations on the similarity profiles for different velocity ratios, with the tanh-profiles.

Next the spatial stability results are presented. The inviscid limit is explored and compared with Michalke (1965). Since the curve of marginal stability must be identical from both the temporal and spatial analyses, comparisons between the two are made for different velocity ratios.

4.4.1 Temporal stability

Note that, if in the Orr–Sommerfeld operator $\mathcal{O}$, $\Phi'(y)$ is identical for all Λ, then a modified definition of the phase-speed

$$\bar{c} = c - \frac{1}{2\Lambda},$$ (4.21)

leads to a modified parallel operator

$$\tilde{\mathcal{O}} = \left(\frac{\Phi'}{2} - \tilde{c}\right)(D^2 - \alpha^2) - \frac{1}{2}\Phi''' - \frac{1}{i\alpha Re}(D^2 - \alpha^2)^2, \qquad (4.22)$$

which is independent of the velocity ratio parameter Λ. Therefore if the curve of marginal stability is given by

$$\tilde{c}_i(\alpha, Re) = 0, \qquad (4.23)$$

then for different velocity ratios this curve remains the same. This is straightforward since the quantity $1/2\Lambda$ modifies only the real-part of c. Hence for the tanh-profile, with Δ and δ_ω as the velocity and length scales respectively, the curve of marginal stability remains the same.

	tanh(any Λ)	$\Lambda = 1/39$	1/3	1
Re = 5	0.000	−0.272	−0.029	−0.086
25	0.000	−0.271	−0.022	−0.062
60	0.000	−0.271	−0.014	−0.040
500	0.000	−0.270	−0.002	−0.008

Table 4.1: Variation of $\tilde{c}_N - \Phi'(0)/2$ along the curve of marginal stability for different velocity-ratios; results from temporal analysis. The rightmost three columns correspond to the similarity solution for the given Λ.

Note that the real-part of the phase speed along the neutral curve, c_N, will change for different values of Λ in the similarity solution. Betchov & Szewczyk (1963) solved the Orr–Sommerfeld equation considering $\Lambda = \infty$ (counterflow) using the tanh profile. It was found that $c_N = 0$ for all (α, Re). Therefore, through the transformation (4.21), we get for all $0 \leq \Lambda \leq 1$, $\tilde{c}_N = 0$. This was verified to be correct up to the specified numerical accuracy. However if the mean flow is given by the similarity solution, then it is expected that this quantity will be different for different Λ. In this case, we make note of the result due to Tollmien (1935) and expect that $\tilde{c}_N - \Phi'(0)/2$ would vanish along the curve of marginal stability. Both
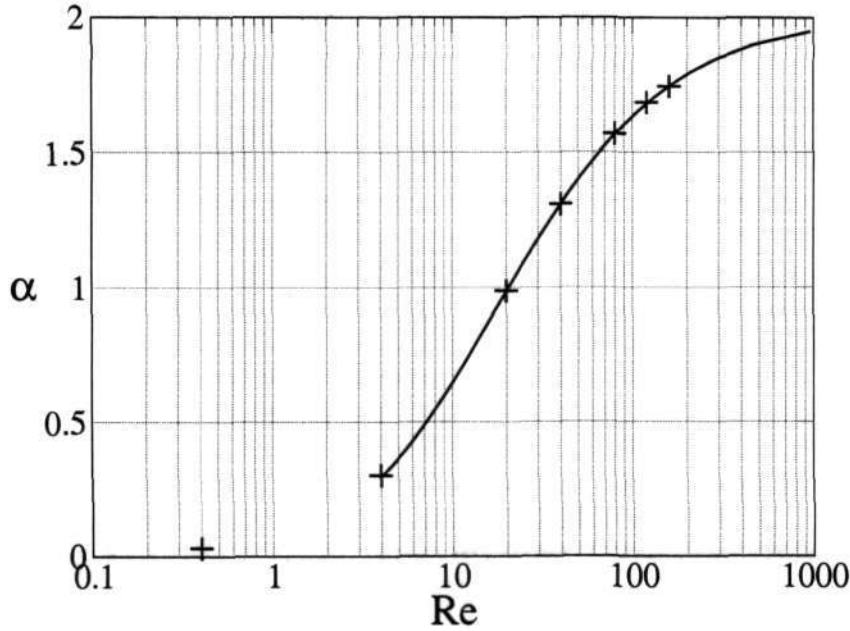
Figure 4.1: Comparison of marginal stability curve from temporal analysis on the tanh $2y$ profile for the case $\Lambda = 1$ (solid line), compared with Betchov & Szewczyk (1963) (circles). Note that in the present calculations, the length and velocity-scales differ from those in Betchov & Szewczyk (1963) by a factor of 2.

these results are presented at indicative values of Re and Λ in table 4.1. Note that for the tanh profile $\Phi'(0) = 0$.

Next, as a benchmarking exercise, we repeat some calculations of Betchov & Szewczyk (1963) for $\Lambda = \infty$ and compare our results with that work. Figure 4.1 compares the marginal stability curve from the present calculation (tanh-profile, temporal stability analysis) with Betchov & Szewczyk (1963). The match is found to be excellent.

Following this, we show the weak dependence of the stability results on the details of the mean-profile. In figure 4.2 the marginal stability curves for $\Lambda = 1$, $1/3$ and $1/39$ are compared, with tanh and the similarity profile as choices for prescribing the mean flow. Note that the asymptotic tendency Re $\rightarrow 0$ of the
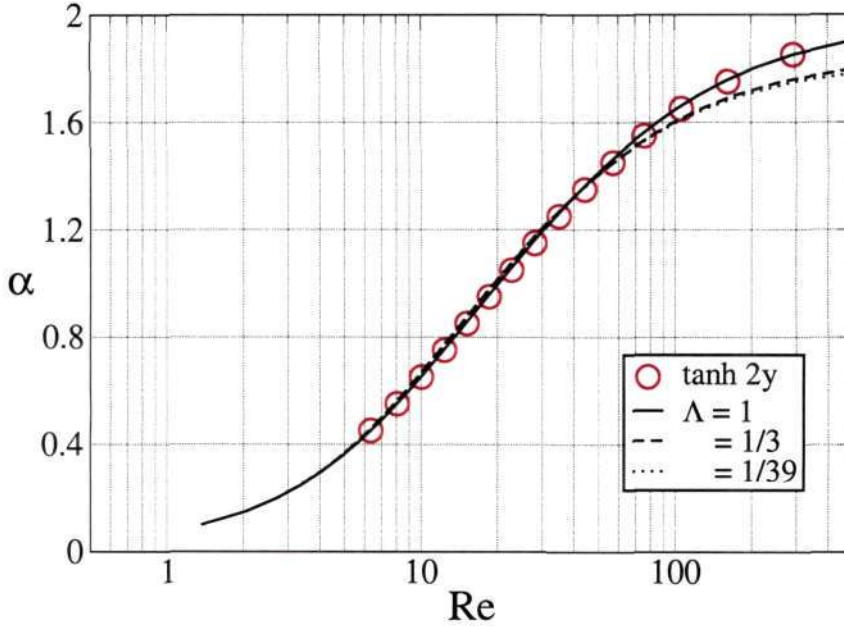
Figure 4.2: Comparison of marginal stability curve from temporal analysis on the tanh $2y$ profile, compared to one with the similarity profile as the mean flow, for $\Lambda = 1$ (halfjet), $\Lambda = 1/3$ and $\Lambda = 1/39$ (nearly shearless flow).

curves is alike. Even for moderate Re (≈ 100), the differences are quite small.

Subsequently, to highlight the effects of the parameters of the analysis, we focus on the case $\Lambda = 1$ (halfjet) with the similarity profile used to prescribe the mean flow. For the limit Re $\rightarrow \infty$ we note that the boundary conditions (3.23) are applicable. This choice is cheaper in terms of computation as a smaller domain is required. However, as Re $\rightarrow 0$, not only does the viscous solution assume larger proportions, but also the wavenumber α decreases monotonically. The decay-rate of the inviscid solution in y being directly proportional to α, larger domain sizes are required at small α for even the inviscid solution to become sufficiently small. In fact, there is an increasingly prohibitive computational cost that must be borne in this limit. This restricted us to obtain definite results only for $\alpha \geq 0.10$.

Two typical points, one in the vanishing Re region ($\alpha = 0.150$) and another

Run	b.c.	L	N	S	α	Re	ω	α	Re	ω
2	(3.23)	8	81	4	0.150	5.441	0.0741	1.000	20.186	0.520
	(3.24)	8	81	4		5.441	0.0741		20.186	0.520
6	(3.23)	16	161	6		2.293	0.0753		20.186	0.520
	(3.24)	16	161	6		2.293	0.0753		20.186	0.520
8	(3.23)	60	201	8		2.047	0.0753		20.186	0.520
	(3.24)	60	201	8		2.048	0.0754		20.186	0.520

Table 4.2: Effect of boundary condition, domain-size and other parameters of the computation. The run number corresponds to that in table 2.1. For all the calculations b was taken equal 0.8.

in the intermediate Re region ($\alpha = 1.000$) of the marginal stability curve are considered. Table 4.2 compares Re and ω for these two α-values. The two boundary conditions (3.23) and (3.24) are compared considering various domain sizes. The results presented in figure 4.2 use parameter values given in the last row of table 4.2.

4.4.2 Spatial analysis

The preceding section analyses the dependence of results on the parameters of the computation. The main conclusion is that a larger domain size L and boundary condition (3.24) need to be used in the Re $\rightarrow$ 0 limit, whereas a smaller domain size and boundary condition (3.23) can be used for intermediate and large Re. The other observations are as follows. Firstly, the stretching factor S and number of grid-points N need to be modified according to the gradient of the eigenfunction near the critical-layer. Secondly, the contracted Howard's semicircle indeed captures the most unstable mode.

Following these results, we do not detail the parametric dependence of results anywhere else in the sequel. Unless otherwise mentioned, the results presented
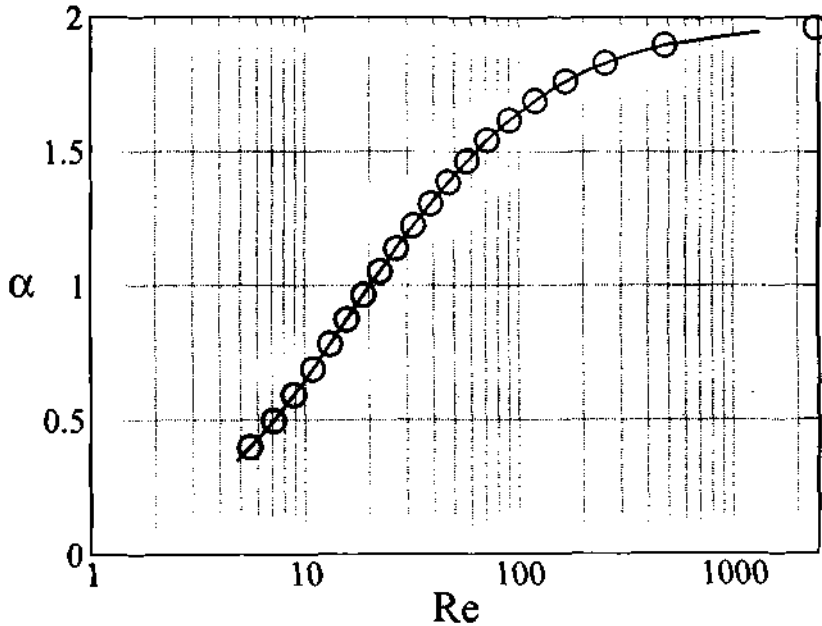
Figure 4.3: Comparison of marginal stability curves from spatial and temporal analyses on the similarity profile for $\Lambda = 1$ (halfjet). Circles, spatial; solid line, temporal (run= 6, $L = 16$, $N = 161$, $S = 6$).

correspond to a judicious choice of parameters, and are sufficiently independent of them. Figures 4.3–4.5 compare the curves of marginal stability (with the similarity solution as the mean flow profile and $\Lambda = 1$, 3/5 and 1/7) from the spatial and temporal stability analyses. The results are found to be indeed indistinguishable, as far as the curve of marginal stability is concerned. Owing to the large size of the matrix that needs to be operated upon for spatial stability calculations ($4N \times 4N$), only indicative points on the marginal curve were computed.

4.5   Conclusions

From the results presented in the preceding section, the following conclusions can be drawn. As expected, the dependence of results on the details of the velocity
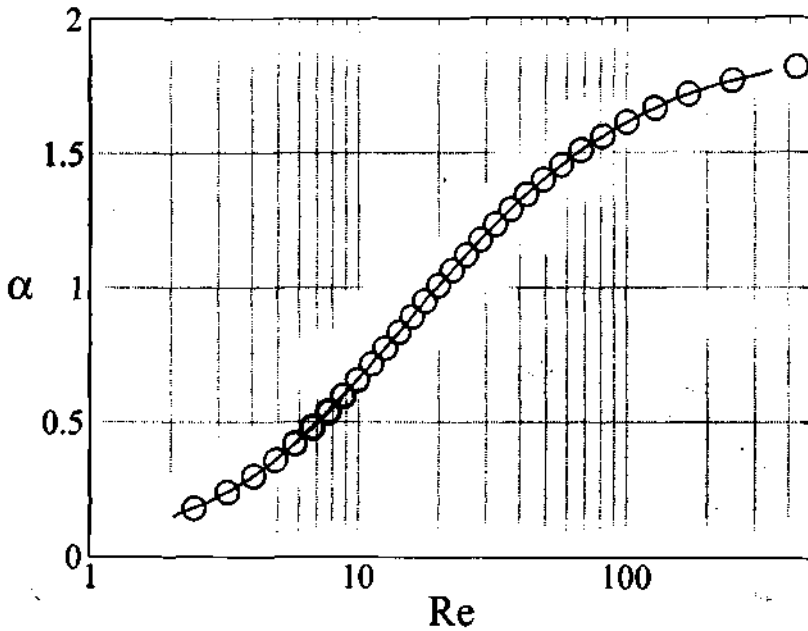
Figure 4.4: Comparison of marginal stability curves from spatial and temporal analyses on the similarity profile for $\Lambda = 3/5$. Circles, spatial; solid line, temporal (run= 10, $L = 60$, $N = 201$, $S = 8$).

profile is indeed weak. Further, spatial and temporal analysis give identical curves of marginal stability. These results are explicitly reported in available literature.

Though parallel stability analysis for all velocity ratios is not reported, we report here that for all velocity ratios considered, a non-zero critical Reynolds number is not found using parallel analysis. Moreover, the vorticity-thickness and the velocity-difference are found to be a judicious choice of scales, the results varying weakly with the velocity-ratio parameter Λ, when expressed in these scales. These lead us to conclude that in the limit $\Lambda \to 0$ (shearless flow), the parallel analysis will predict instability for all Reynolds number. (The case of nearly shearless flow, $\Lambda = 1/39$, quite illustrates the point.)

The last statement is quite counter-intuitive – and in fact meaningless – because in the absence of a velocity-gradient, or shear (the sole agent of energy transfer
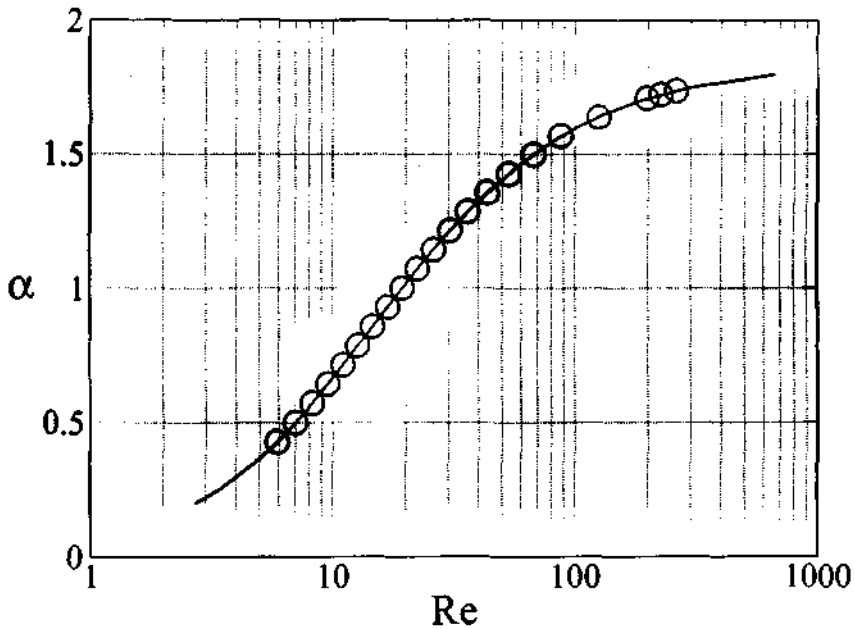
Figure 4.5: Comparison of marginal stability curves from spatial and temporal analyses on the similarity profile for $\Lambda = 1/7$. Circles, spatial; solid line, temporal (run= 12, $L = 60$, $N = 201$, $S = 8$).

between the mean flow and the perturbation-field), one would expect the flow to be stable. As noted earlier, parallel analysis is valid as long as the local thickness is constant, that is it does not change appreciably over one wavelength of the disturbance mode. By implication this leads to the conclusion that for a fixed δ_ω, the flow remains unstable as $\Delta \rightarrow 0$. This is seen as a major failure of parallel-flow theory.

CHAPTER 5

MINIMAL COMPOSITE (NON-PARALLEL) THEORY

In the preceding chapter it was noted that parallel-flow theory gives an unphysical result of $\mathrm{Re}_c = 0$ for the plane mixing layer for all velocity ratios. That is to say there exists no Reynolds number, below which the gain in the disturbance kinetic energy moving downstream is outdone by loss to viscous dissipation. Kundu & Cohen (2005, pp. 478–480) show that, in a parallel flow, the integral of disturbance kinetic-energy taken over a control volume $\mathcal{V}$, which is a slab of infinitesimal thickness at a particular streamwise location and extending throughout the whole of the normal domain (see figure 5.1), has its growth rate given by the difference of two quantities,

$$\frac{\mathrm{d}}{\mathrm{d}t_d} \int \frac{1}{2}(u_d^2 + v_d^2)\mathrm{d}\mathcal{V} = -\int u_d v_d \frac{\partial U_d}{\partial y_d}\mathrm{d}\mathcal{V} - \varepsilon, \qquad (5.1)$$

where ε is the rate of viscous dissipation in the control volume $\mathcal{V}$. The simple interpretation of this equation is as follows. For two-dimensional disturbances in a parallel shear flow the decay or growth of disturbances is a difference of the net production and the net dissipation. The production is an effect of inertia of the flow and the dissipation is related to viscosity. The rest of the quantities, contributing locally to the growth or decay, sum to zero when integrated over a control volume like in figure 5.1. This can be attributed to the fact that these other terms can be

43

written as gradients of quantities that vanish at the boundary of the control-volume and from the Gauss divergence theorem the result follows. For non-parallel flows the expressions for production and dissipation contain more terms than in (5.1) but the integral energy balance is between these two quantities alone.
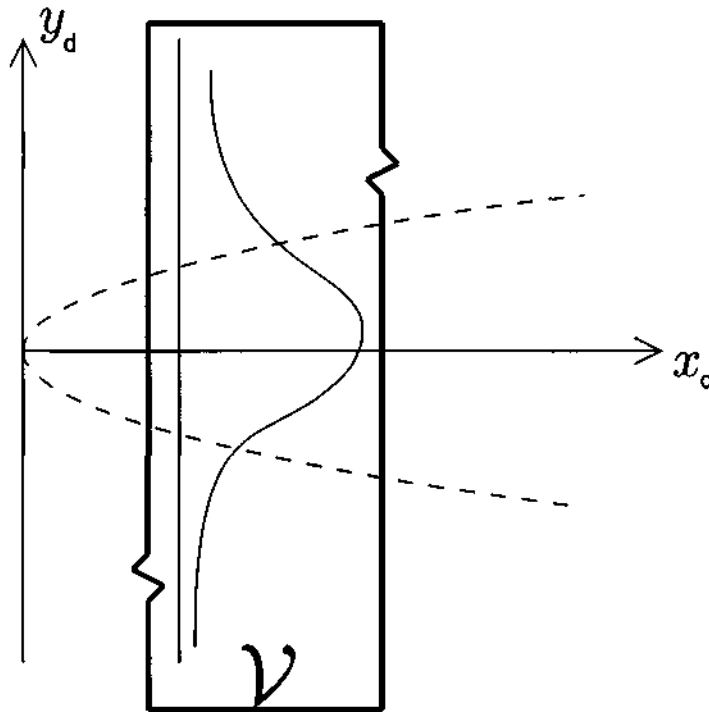
Figure 5.1: Integral of the disturbance kinetic energy over a control volume extending throughout the y_d-domain, taken at a particular x_d-location.

The result from Orr–Sommerfeld analysis that the difference between production and dissipation the two is never negative (which would signify decay), whatever the Reynolds number, is contradictory to what is known from other energy theories applicable to two-dimensional shear flows of which the mixing layer is one instance. In fact, Lin (1955), Lorentz (1907), Joseph (1966) assert that a finite Reynolds number, however small, must exist below which viscosity dampens out

the growth of infinitesimally small perturbations.

Indeed, Cowley & Wu (1994) call the Reynolds number in Orr–Sommerfeld-like theories schizophrenic. From our earlier discussion, recall that Orr–Sommerfeld is an ad-hoc equation for non-parallel flow insofar that it does not represent the Navier–Stokes asymptotically at any finite Re except in parallel flows. Further, in the case of the mixing layer, the curve of marginal stability traverses regimes of very low Re (see previous chapter), where the penalty of neglecting non-parallelism becomes acute. Recall that the quantity p/Re in equation (3.2) mathematically accounts for the fact that the mixing layer is highly non-parallel at low Re. Whether non-parallel theory is able to resolve the problem of zero critical Reynolds number needs to be investigated, but it must be conceded at the outset that the result from the parallel theory must be rejected near $\text{Re} = 0$ for the mixing layer.

A theory that can replace Orr–Sommerfeld, therefore, must take the effect of viscosity into account consistently. Further this theory should pose the problem in a manner that retains some amount of mathematical tractability. In this chapter the minimal composite theory, developed in Govindarajan & Narasimha (1995, 1997) is applied to the mixing layer.

5.1   Background

In the linear stability analysis of the boundary layer, which has received a significant part of the attention directed to the development of non-parallel theories, it was well known very early on (Bouthier, 1972, 1973; Gaster, 1974; Saric & Nayfeh, 1975) that to reconcile the theory to experimental observation, non-parallel effects cannot be neglected. Various workers have tried to include effects of flow non-parallelism into parallel theory. One idea that was introduced was that the mean flow must

be specified to a higher-order to obtain non-parallel effects. The rationale behind this was that flow non-parallelism, that can be quantified using p/Re, is a higher order effect in what is typically a large Re flow situation.

Govindarajan & Narasimha (1995, 1997) discuss the work of previous workers where attempts were made to include higher order terms, the different formulations that were arrived at, and the results from these. However, it was argued by Govindarajan & Narasimha (1995, 1997) that in the case of boundary layers, non-parallel effects could already be traced to lower orders than $O\left(\text{Re}^{-1}\right)$. It was further argued that to obtain the lowest order non-parallel effects, higher order corrections to the mean flow specification were unnecessary. This led to the minimal equation in Govindarajan & Narasimha (1997) that uses similarity variables and follows from a lowest order rational asymptotic theory correct up to (but not including) $O(\text{Re}^{-2/3})$, where Re is the local Reynolds number based on, say, the momentum thickness of the boundary layer.

Though this equation is an ordinary differential equation in y, it inherently carries the non-parallel information through the local length-scale (the momentum thickness, for instance), based on which y is non-dimensionalized. It was shown that the minimal equation could replace the ad-hoc Orr–Sommerfeld equation in providing a rational description of the flow correct to the lowest order. Further, the solution to this equation was seen to capture all the non-parallel effects (for e.g., the zero crossing of the disturbance streamfunction at a y-location close to the wall) that can be obtained from higher order theories.

Further development along this line of work was introduced in Govindarajan & Narasimha (2005) where the minimal composite equation formulated in Govindarajan & Narasimha (1997), was shown to be sufficient to calculate spatial growth rates correct to $O\left(\text{Re}^{-1}\right)$. This is indeed non-trivial because the minimal composite

equation is correct only up to (but not including) $O(\mathrm{Re}^{-2/3})$. To achieve this level of accuracy, the property of adjoints was used to obtain the contribution to the non-parallel growth rate from the cumulative streamwise change in the structure of the streamfunction and its magnitude. A formally introduced "slowly varying" amplitude function absorbed the $O(1)$ changes in the shape of the streamfunction. Govindarajan & Narasimha (2005) applied this method to boundary layers, reporting results correct to 3% to those obtained from full non-parallel theory in predicting the amplitude ratio, even in strong adverse pressure gradients.

In the following sections, the full minimal composite machinery is developed for the mixing layer problem and the formulation to compute the growth rate correct to $O\left(\mathrm{Re}^{-1}\right)$ is presented.

5.2 Principles

Unlike in the Orr-Sommerfeld equation, V_d and $\partial U_d/\partial x_d$ are now not dropped from the equations of evolution for the infinitesimal disturbances. In fact, all the mean flow terms are retained at the start of the analysis. The linearized equations for two-dimensional disturbances are

$$\frac{\partial u_d}{\partial x_d} + \frac{\partial v_d}{\partial y_d} = 0, \tag{5.2}$$

$$\begin{aligned}\frac{\partial u_d}{\partial t_d} + U_d\frac{\partial u_d}{\partial x_d} + u_d\frac{\partial U_d}{\partial x_d} & \\ + V_d\frac{\partial u_d}{\partial y_d} + v_d\frac{\partial U_d}{\partial y_d} &= -\frac{1}{\rho}\frac{\partial \Pi_d}{\partial x_d} + \nu\nabla_{\mathrm{H}}^2 u_d,\end{aligned} \tag{5.3}$$

$$\begin{aligned}\text{and}\quad \frac{\partial v_d}{\partial t_d} + U_d\frac{\partial v_d}{\partial x_d} + u_d\frac{\partial V_d}{\partial x_d} & \\ + V_d\frac{\partial v_d}{\partial y_d} + v_d\frac{\partial V_d}{\partial y_d} &= -\frac{1}{\rho}\frac{\partial \Pi_d}{\partial y_d} + \nu\nabla_{\mathrm{H}}^2 v_d,\end{aligned} \tag{5.4}$$

where $\nabla_H^2 = \partial^2/\partial x_d^2 + \partial^2/\partial y_d^2$. We consider only two-dimensional disturbances, assuming the result due to Squire (1933) to hold. The theorem is not proven for the non-parallel case but experimental evidence lends support to our ansatz. It is noted there that the initial breakdown is predominantly two-dimensional (Metcalfe, Orszag, Brachet, Menon & Riley, 1987).

Fully non-parallel theory is constructed as a development over an underlying *consistently* lowest-order theory which substitutes for the inconsistent parallel theory. Following parallel analysis, we seek wavelike solutions to the perturbation streamfunction and pressure of the form

$$\{\phi_d, \Pi_d\} = \{\hat{\phi}_d(x_d, y_d), \hat{p}_d(x_d, y_d)\} \exp\left[i\left(\int_{x_0}^x \alpha \, dx - \omega t\right)\right], \qquad (5.5)$$

where ω is the pure-real frequency, α is the full-complex wavenumber, and x_0 corresponds to some reference location with respect to which the growth and phase are monitored. Note that in experiments the dimensional frequency ω_d is a constant which is simply the frequency of a vibrating ribbon that produces the perturbation. To non-dimensionalize, we use the length and velocity scales δ_ω and Δ as follows

$$\left.\begin{array}{rclcrcl}
dx_d &=& \delta_\omega dx, & & y_d &=& \delta_\omega y, \\[4pt]
t_d &=& \delta_\omega t/\Delta, & & \alpha_d &=& \alpha(x)/\delta_\omega, \\[4pt]
\omega_d &=& \omega\Delta/\delta_\omega, & & \hat{\phi}_d &=& (\delta_\omega\Delta)\hat{\phi}(x,y), \\[4pt]
\text{and} \quad \hat{p}_d &=& (\rho\Delta^2/2)\hat{p}(x,y). & & & &
\end{array}\right\} \qquad (5.6)$$

Here, the d-subscripted quantities are dimensional. Note that since the mean flow varies in the streamwise direction, the coefficients of the operator governing the evolution of disturbance quantities in (5.3) and (5.4) are also x_d-dependent. Therefore the dispersion relation between ω and α is not invariant in x. Hence α also is taken

to be a function of x. Similarly the amplitudes of streamfunction $\hat{\phi}$ and pressure $\hat{p}$ are also x-dependent. It must be emphasized here that δ_ω is not any arbitrary constant like in (3.9) but is given by (3.2). Moreover the streamwise distance x is made dimensionless in a different manner compared to that in (3.9).

Next we make an assumption that is central to the mathematical tractability of the problem. We assume that for all the wavelike features, namely the amplitudes of streamfunction $\hat{\phi}$ and pressure $\hat{p}$, and the wavenumber α, changes over a characteristic distance in the streamwise direction are small. That is, assuming $\hat{\phi}, \alpha$ to be $O(1)$ we insist that

$$\frac{\partial \hat{\phi}}{\partial x}, \frac{\partial \alpha}{\partial x} \sim \frac{1}{x} \sim O\left(\mathrm{Re}^{-1}\right). \tag{5.7}$$

From (3.2) and (5.6) we note that the above condition restricts the rate of streamwise variation of the wave-features to the same order of magnitude as the local rate of growth of the vorticity-thickness. This assumption can be verified only a posteriori, i. e. after the results have been obtained.

5.3 Order of magnitude analysis

We introduce the perturbation streamfunction (5.5) that automatically satisfies (5.2) into the curl of the equations (5.3) and (5.4). This gives

$$
\begin{aligned}
\frac{\partial}{\partial t_d}\left(\nabla_{\mathrm{H}}^2 \phi_d\right) &+ \left(U_d \frac{\partial}{\partial x_d} + V_d \frac{\partial}{\partial y_d}\right) \nabla_{\mathrm{H}}^2 \phi_d \\
&+ \left(\frac{\partial^2 U_d}{\partial y_d \partial x_d} - \frac{\partial^2 V_d}{\partial x_d^2}\right) \frac{\partial \phi_d}{\partial y_d} \\
&- \left(\frac{\partial^2 U_d}{\partial y_d^2} - \frac{\partial^2 V_d}{\partial x_d \partial y_d}\right) \frac{\partial \phi_d}{\partial x_d} = \nu \nabla_{\mathrm{H}}^2 \nabla_{\mathrm{H}}^2 \phi_d.
\end{aligned} \tag{5.8}
$$

Substituting (2.15), (5.5) and (5.6) into (5.8), and dropping all terms smaller than $O\left(\mathrm{Re}^{-1}\right)$ (see Appendix A for details), we get (employing the assumption (5.7))

$$\mathcal{N}\hat{\phi} = o(\mathrm{Re}^{-1}),\tag{5.9}$$

where

$$
\begin{aligned}
\mathcal{N} \equiv\ & \left(\frac{1}{2\Lambda} + \frac{\Phi'}{2} - c\right)(\mathrm{D}^2 - \alpha^2) - \frac{1}{2}\Phi''' \\
& - \frac{1}{i\alpha\mathrm{Re}}\left\{(\mathrm{D}^2 - \alpha^2)^2 + p\left(\frac{\Phi}{2} + \frac{y}{2\Lambda}\right)\mathrm{D}^3\right. \\
& + p\left[\left(\frac{1}{2\Lambda} + \frac{\Phi'}{2}\right)\mathrm{D}^2 + \frac{\Phi''}{2}\mathrm{D}\right] - p\alpha^2 c + p\frac{\Phi'''}{2} \\
& - \alpha^2\left[2py\left(\frac{1}{2\Lambda} + \frac{\Phi'}{2} - c\right) + p\left(\frac{\Phi}{2} + \frac{y}{2\Lambda}\right)\right]\mathrm{D} \\
& + \left.\left[3\left(\frac{\Phi'}{2} + \frac{1}{2\Lambda}\right) - c\right]\mathrm{Re}\alpha\alpha' + \mathcal{S}\mathrm{Re}\frac{\partial}{\partial x}\right\},
\end{aligned}\tag{5.10}
$$

$$\mathcal{S} \equiv \frac{\Phi'''}{2} - \left(\frac{\Phi'}{2} + \frac{1}{2\Lambda}\right)\mathrm{D}^2 + \alpha^2\left[3\left(\frac{\Phi'}{2} + \frac{1}{2\Lambda}\right) - 2c\right]\tag{5.11}$$

and $\alpha' = \partial\alpha/\partial x$.

The operator $\mathcal{N}$ is the mixing-layer counterpart of the operator $\{\mathrm{NP}\}$ appearing in Govindarajan & Narasimha (1995), where it was derived for the boundary-layer over a flat-plate. This operator contains all terms nominally correct to $O\left(\mathrm{Re}^{-1}\right)$. It is shown in Govindarajan & Narasimha (2001) that $\mathcal{N}$ forms a subset of the operator governing the parabolized stability equations (PSE) (Herbert, 1997), omitting those that are $o(\mathrm{Re}^{-1})$, and is also equivalent to the formulation by Gaster (1974). There are several differences between $\mathcal{N}$ and $\mathcal{O}$. Firstly, we note that the similarity streamfunction Φ scaled by the local vorticity-thickness δ_ω enters $\mathcal{N}$ instead of the parallel profile $U_d(y_d)$. Thus the normal coordinate y is the similarity variable and not merely a non-dimensional coordinate scaled by an invariant length (such as

ν/U_∞). The dependence of δ_ω on x_d is factored in through terms with coefficients containing p.

However, note that the viscous diffusion contribution is exactly the same in both $\mathcal{N}$ and $\mathcal{O}$. This is to be expected since the viscous diffusion terms in $\mathcal{O}$ already have a factor Re^{-1} multiplying them. Thus higher-order contributions due to streamwise derivatives in viscous terms must be rejected in $\mathcal{N}$ too.

The rationale behind retaining terms upto $O\left(\mathrm{Re}^{-1}\right)$ is the following. The mean flow is obtained from the similarity solution which satisfies the Navier–Stokes equations correct to $O\left(\mathrm{Re}^{-1}\right)$. Now to get the perturbation field correct to an order higher than Re^{-1}, we need an equation governing it correct to such an order. This equation will need to include the mean flow correct to an order higher than Re^{-1}. However, it was argued in Govindarajan & Narasimha (1997) that there is no basis to claim that non-parallel effects can be incorporated only by including higher order mean flow effets. This is once again obvious from (5.10), where we already have non-parallel terms included along with parallel contributions, without needing to compute higher-order solutions to the mean flow. Thus restricting the analysis to $O\left(\mathrm{Re}^{-1}\right)$ is sufficient to include the lowest-order non-parallel effects.

Again, it must be emphasized that the use of the similarity solution allows us to separate terms of different orders. This would not have been feasible if a numerical solution of the full Navier–Stokes was used to prescribe the mean flow. As was pointed out in Govindarajan & Narasimha (1995), it is the use of the similarity law that allows omitting higher-order terms appearing in the PSE without losing consistency in the analysis upto $O\left(\mathrm{Re}^{-1}\right)$.

Following Govindarajan & Narasimha (1997), we look for the lowest-order solution to (5.9) insisting on a rational, asymptotically valid formulation. It is expected that the terms with streamwise derivatives would not contribute directly at

the lowest-order, but eventually will need to be accounted for if it is to be different from parallel theory. In Govindarajan & Narasimha (1995), $\mathcal{N}$ was solved completely, but further analysis developed in Govindarajan & Narasimha (2005) shows that the lowest-order equation alone can be used to determine the non-parallel growth-rate of disturbance correct to $O\left(\mathrm{Re}^{-1}\right)$.

5.4   Minimal composite operator

We consider the dynamics in the far field, where $y \sim O(1)$, such that $\mathrm{D} \sim O(1)$. All viscous terms need to be dropped, since they contain an explicit Re^{-1} factor. Similarly all terms that scale as $O\left(\mathrm{Re}^{-1}\right)$ are omitted. This gives the lowest-order operator at large y

$$\mathcal{M}_\infty = \left(\frac{1}{2\Lambda} + \frac{\Phi'}{2} - c\right)(\mathrm{D}^2 - \alpha^2) - \frac{1}{2}\Phi''', \qquad y \sim O(1). \qquad (5.12)$$

This operator is expectedly identical to the Rayleigh operator and suffers from the same problem of singularity at the critical point y_c. In Narasimha & Govindarajan (2000) it was commented that (5.12) determines the flow in the bulk, given by a fixed y and with $\mathrm{Re} \to \infty$; or for a fixed Re, with $y \to \infty$.

In § 4.4.1, it was noted that $y_c \approx y_s = 0$, and therefore

$$\Phi_c, \, \Phi_c''' \approx 0. \qquad (5.13)$$

Now, expanding the mean flow streamfunction and the streamwise velocity near

the critical point y_c we get, for $y \to y_c$,

$$\Phi(y) = [2c_r - (1/\Lambda)]y + \Phi_c'' \frac{y^2}{2!} + O(y^4), \qquad (5.14)$$

$$\text{and} \quad \Phi'(y) = [2c_r - (1/\Lambda)] + \Phi_c'' y + O(y^3), \qquad (5.15)$$

where the subscript c denotes the value of the quantity evaluated at the critical point. The y-derivatives D^n are expected to scale as δ_c^{-n}, where δ_c is the characteristic thickness of the critical layer. Therefore, the lowest-order balance at $y \sim O(\delta_c)$ gives

$$\mathcal{M}_c = \left(\frac{\Phi'}{2} + \frac{1}{2\Lambda} - c \right) D^2 - \frac{1}{i\alpha Re} D^4 - \frac{1}{2} \Phi''', \qquad (5.16)$$

$$\text{and} \quad \delta_c \sim O(\alpha Re)^{-1/3}. \qquad (5.17)$$

(It has been assumed that Φ_c'' is $O(1)$.) If a matched asymptotic expansion technique were to be employed, a strategy for matching the solution to (5.12) (*outer* solution) with the solution to (5.16) (*inner* solution) would be needed to be specified at this stage. But we intend to solve for the lowest-order solution numerically. Thus it only needs to be ensured that the operator governing it contains all terms that are required to match the solution in different distinguished limits. Note the absence of a wall-layer analysis. For the general case of a flow with a solid boundary, the viscous wall-layer analysis as given in Narasimha & Govindarajan (2000) needs to be carried out.

Following this scheme, we compose the minimal equation needed to obtain the lowest-order solution $\hat{\phi}_m$, given by

$$\mathcal{M} \hat{\phi}_m = 0, \qquad (5.18)$$

where

$$\mathcal{M} \equiv \left(\frac{\Phi'}{2} + \frac{1}{2\Lambda} - c \right) (D^2 - \alpha^2) - \frac{1}{i\alpha Re} D^4 - \frac{1}{2} \Phi''', \qquad (5.19)$$

which is simply the superset of $\mathcal{M}_\infty$ and $\mathcal{M}_c$. Note that the critical layer analysis gives the thickness of the critical layer δ_c in terms of the product (αRe). Using $\mathcal{M}$, we are ready to solve for the lowest-order eigenfunction $\hat{\phi}_m$ at a given Re. The eigenfunction is scaled by the local vorticity-thickness which is also included in Re.

At this point it is useful to define the higher-order operator $\mathcal{H}$ which contains all the terms in $\mathcal{N}$ that are omitted in $\mathcal{M}$:

$$\begin{aligned}
\mathcal{H} \equiv \ & -\frac{1}{i\alpha Re} \left\{ \alpha^4 - 2\alpha^2 D^2 + p \left(\frac{\Phi}{2} + \frac{y}{2\Lambda} \right) D^3 \right. \\
& + p \left[\left(\frac{1}{2\Lambda} + \frac{\Phi'}{2} \right) D^2 + \frac{\Phi''}{2} D \right] - p\alpha^2 c + p \frac{\Phi'''}{2} \\
& - \alpha^2 \left[2py \left(\frac{1}{2\Lambda} + \frac{\Phi'}{2} - c \right) + p \left(\frac{\Phi}{2} + \frac{y}{2\Lambda} \right) \right] D \\
& \left. + \left[3 \left(\frac{\Phi'}{2} + \frac{1}{2\Lambda} \right) - c \right] Re\alpha\alpha' + \mathcal{S}Re \frac{\partial}{\partial x} \right\}.
\end{aligned} \qquad (5.20)$$

Note that, unlike in $\mathcal{O}$, not all the viscous diffusion terms make it to $\mathcal{M}$, even in the critical layer. To compose $\mathcal{M}$, care is taken to include terms only to a *distinguished* limit. With the prescription of the mean flow using the similarity solution the operator $\mathcal{M}$, unlike $\mathcal{O}$, is therefore a consistent lowest-order operator.

Further observe that $\mathcal{M}$ does not contain any x-derivative. Therefore if any complex-valued function $A(x)$ is multiplied to the lowest-order eigenfunction $\hat{\phi}_m$, the resulting function also satisfies $\mathcal{M}$. $A(x)$ is called the amplitude function and following our slowly-varying precondition for the wave-like solutions, we insist that $(1/A)(dA/dx)$ is at the most $O\left(Re^{-1}\right)$. Next we express the total solution $\hat{\phi}$ into

a lowest-order solution $\hat{\phi}_m$ and higher-order correction $\hat{\phi}_h$ as

$$\hat{\phi} = A\hat{\phi}_m + \epsilon\hat{\phi}_h, \tag{5.21}$$

where ϵ is the order at which $\hat{\phi}_h$ makes a contribution to $\hat{\phi}$. Now, terms in $\mathcal{H}$ attain different orders of magnitude, both compared to each other, as well as at different regions in the y-domain. The largest of all these various magnitudes is the lowest-order neglected in $\mathcal{M}$, and therefore in computing $\hat{\phi}_m$. Therefore the correction to $\hat{\phi}_m$ must also be of the same order. From (5.20), it is seen that the $-(p/i\alpha\mathrm{Re})[(1/2\Lambda) + (\Phi'/2)]\mathrm{D}^2$ and $-(p/i\alpha\mathrm{Re})[(y/2\Lambda) + (\Phi/2)]\mathrm{D}^3$ terms are $O(\alpha\mathrm{Re})^{-2/3}$ compared to the lowest order term in the critical layer, makes the largest contribution to $\mathcal{H}$. Evidently thus

$$\epsilon \sim O(\alpha\mathrm{Re})^{-2/3}. \tag{5.22}$$

Again, it is emphasized that it is not our objective to obtain the higher-order solution $\hat{\phi}_h$ after $\hat{\phi}_m$ has been obtained. Instead, the focus of the sequel is on defining the growth-rate using which the curve of marginal stability can be computed.

5.5   Non-parallel growth-rate

It is well-known in non-parallel theory that the growth-rate depends upon a number of factors. Assume a perturbation quantity q_d of the form

$$q_d = \hat{q}_d(x, y) \exp\left[i \left(\int_{x_0}^{x} \alpha \, dx - \omega t \right) \right]. \tag{5.23}$$

The growth-rate of this quantity in the streamwise direction is defined as

$$g \equiv \left(\frac{\delta_\omega}{q_d} \frac{\partial q_d}{\partial x_d} \right)_r. \qquad (5.24)$$

Now, assume a non-dimensionalization of $\hat{q}_d$ as follows

$$\hat{q}_d = \delta_\omega^a \Delta^b \hat{q}(x, y). \qquad (5.25)$$

where a and b are some constants. Without loss of generality, following our asymptotic expansion it is expected that $\hat{q}$ will have contributions at the lowest-order and from subsequent higher orders. The lowest-order contribution can be expressed in terms of the lowest-order streamfunction $\hat{\phi}_m$ as it describes the flow correctly in the corresponding limit. To express $\hat{q}$ correct to any subsequent higher order, information is needed from all orders lower and upto that order. This follows from standard asymptotic theory.

From the discussion above, we split $\hat{q}$ into lowest and higher-order contributions. Moreover, as noted previously, all calculations are at best correct upto $O\left(\text{Re}^{-1}\right)$. Therefore $\hat{q}$ also cannot be evaluated correct to any order higher than $O\left(\text{Re}^{-1}\right)$. Hence we write

$$\hat{q} = \hat{q}_m(x, y) + \epsilon \hat{q}_h(x, y). \qquad (5.26)$$

From (5.24) the growth-rate correct to $O\left(\text{Re}^{-1}\right)$ is therefore given by

$$g = -\alpha_i + \frac{1}{\hat{q}_m} \frac{\partial \hat{q}_m}{\partial x} - \frac{py}{\text{Re}} \frac{D\hat{q}_m}{\hat{q}_m} + a\frac{p}{\text{Re}}. \qquad (5.27)$$

Now it is straightforward to appreciate how the non-parallelism manifests itself. Comparing (5.27) with (3.26) we find that the non-parallel contributions to the

growth rate are

$$g_{np} = \frac{1}{\hat{q}_m} \frac{\partial \hat{q}_m}{\partial x} - \frac{py}{\mathrm{Re}} \frac{\mathrm{D}\hat{q}_m}{\hat{q}_m} + a\frac{p}{\mathrm{Re}}. \tag{5.28}$$

It is interesting to note that the rate of spreading of the mixing layer, which is given by the p/Re term, makes a contribution opposite or identical in sign to the parallel growth rate α_i, depending on the sign of a. Lessen & Ko (1966) were thus incorrect in assuming a simple and unqualified relationship, which in the present variables reads

$$g = -\alpha_i - \frac{p}{\mathrm{Re}}.$$

For the mixing layer, which is highly non-parallel at low Reynolds numbers (indicated by the fact that p/Re becomes large), the sign of a may play a decisive role in determining the stability behaviour of the quantity q_d in question. Also the fact that the eigenfunction $\hat{\phi}_m$ is x-dependent needs to be considered. To summarize, the growth-rate g in (5.27) depends on

- the quantity being monitored,

- the y-location where it is evaluated, and

- the local degree of non-parallelism.

5.6 Method of adjoints

Gaster (1974) first applied the method of adjoints to the solutions of the ordinary differential equation (the Orr–Sommerfeld equation in his case), to obtain a growth rate with contributions at higher order than terms neglected in the ordinary differential equation. Govindarajan & Narasimha (2005) started with the minimal

composite equation for the boundary layer, instead of the Orr–Sommerfeld equation, to the same effect. Here we essentially follow the latter approach and apply it to the mixing layer. To compute g from (5.27), the following procedure is used. Equation (5.18) is solved with boundary conditions (3.17) for a given ω_d and Re, to obtain α and $\hat{\phi}_m$. We denote this solution by $\alpha(\text{Re})$ and $\hat{\phi}_m(\text{Re})$. Therefore the first term and the last two terms in the right hand side of (5.27) are known. To compute the second term, whatever be the choice of q_d, it is necessary to evaluate the quantities $\partial\hat{\phi}_m/\partial x$ and $(1/A)(\mathrm{d}A/\mathrm{d}x)$. The first of these is evaluated using a first-order forward-difference

$$\frac{\partial\hat{\phi}_m}{\partial x} = \frac{\hat{\phi}_m(\text{Re} + \delta\text{Re}) - \hat{\phi}_m(\text{Re})}{(\delta\text{Re}/p)}, \tag{5.29}$$

where $\hat{\phi}_m(\text{Re} + \delta\text{Re})$ is the solution to (5.18) with boundary conditions (3.17), for the same ω_d as above but with the Reynolds number equal to $\text{Re} + \delta\text{Re}$. The wavenumber corresponding to $\hat{\phi}_m(\text{Re} + \delta\text{Re})$ is denoted by $\alpha(\text{Re} + \delta\text{Re})$. Here δRe is taken sufficiently small such that the results are independent of δRe to at least within the computational accuracy. Recall that $\mathrm{d}x = \mathrm{d}\text{Re}/p$, from (2.16), (3.2) and (5.6). A similar scheme is used to calculate the quantity α'.

To compute $(1/A)(\mathrm{d}A/\mathrm{d}x)$, we substitute (5.21) into (5.9) to get

$$A\mathcal{H}\hat{\phi}_m - \frac{1}{\mathrm{i}\alpha}\frac{\mathrm{d}A}{\mathrm{d}x}\mathcal{S}\hat{\phi}_m + \epsilon\mathcal{M}\hat{\phi}_h = o(\text{Re}^{-1}), \tag{5.30}$$

where (5.18) has been used. Now consider the adjoint of the operator $\mathcal{M}$

$$\mathcal{M}^\dagger = \left(\frac{\Phi'}{2} + \frac{1}{2\Lambda} - c^*\right)(\mathrm{D}^2 - \alpha^{*2}) + \frac{1}{\mathrm{i}\alpha^*\text{Re}}\mathrm{D}^4 + \Phi''\mathrm{D}, \tag{5.31}$$

where the asterisk denotes the complex-conjugate. Here the adjoint of a linear

operator $\mathcal{L}$ with complex-valued coefficients $w_j(y)$ and operating on a function $\phi(y)$

$$\mathcal{L}\phi = (w_0 D^4 + w_1 D^3 + \cdots + w_4)\phi,$$

is defined as follows,

$$\mathcal{L}^\dagger \phi \equiv D^4(w_0^* \phi) - D^3(w_1^* \phi) + \cdots + (-1)^4 w_4 \phi.$$

Further, from the property of adjoints, for any two functions ρ and σ satisfying the same boundary conditions,

$$\int_{-\infty}^{\infty} \sigma^* \mathcal{M} \rho \, dy = \int_{-\infty}^{\infty} \rho^* \mathcal{M}^\dagger \sigma \, dy. \tag{5.32}$$

Now, if $\hat{\chi}$ satisfies

$$\mathcal{M}^\dagger \hat{\chi} = 0 \tag{5.33}$$

with boundary conditions (3.17), then from (5.32) it follows that

$$\int_{-\infty}^{\infty} \hat{\chi}^* \mathcal{M} \hat{\phi}_h \, dy = \int_{-\infty}^{\infty} \hat{\phi}_h^* \mathcal{M}^\dagger \hat{\chi} \, dy = 0. \tag{5.34}$$

Here we have used (5.33) and the fact that $\hat{\phi}_h$ satisfies (3.17). Now multiplying $\hat{\chi}^*$ into both sides of (5.30) and integrating we obtain

$$\frac{1}{A} \frac{dA}{dx} = i\alpha \frac{\displaystyle\int_{-\infty}^{\infty} \hat{\chi}^* \mathcal{H} \hat{\phi}_m \, dy}{\displaystyle\int_{-\infty}^{\infty} \hat{\chi}^* \mathcal{S} \hat{\phi}_m \, dy}. \tag{5.35}$$

The lowest-order solution $\hat{\phi}_m$ being known at Re, as well as the quantities $\partial \hat{\phi}_m / \partial x$ and α' from (5.29) and a similar procedure, as soon as $\hat{\chi}$ is computed, identity (5.35)

can be used to calculate $(1/A)(dA/dx)$ and consequently g in (5.27), to an accuracy

of $o(\mathrm{Re}^{-1})$. To determine $\hat{\chi}$, equation (5.33) is solved with $\mathcal{M}^{\dagger}$ using ω_d, Re and

$\alpha(\mathrm{Re})$.

A comment regarding the choice of normalization of the eigenfunction $\hat{\phi}_m$ needs

to be made. Suppose a certain normalization scheme is chosen. From (5.29)

and (5.35), the quantities $\partial\hat{\phi}_m/\partial x$ and $(1/A)(dA/dx)$ will have certain values.

If the normalization scheme is changed, it is expected that these quantities will

now have different values. Fasel & Konzelmann (1990) argued that whatever be

the normalization scheme, the sum of both these contributions always remains the

same. Therefore the stability result is independent of the normalization. However,

if the contributions are to be separately compared, then the normalization must

be consistent throughout.

CHAPTER 6

NON-PARALLEL STABILITY ANALYSIS

In this chapter the spatial stability analysis of the mixing layer, based on the minimal composite theory presented in the foregoing, is undertaken. A disturbance mode, identified by its dimensional frequency ω_d, is introduced into the mean flow. For various physical disturbance quantities, growth-rates and hence stability boundaries are defined. Parameters of the computation and tolerances are specified where they occur.

6.1 Real part of waveform

The generalised definition of the growth-rate (5.24) leading to (5.27) suffices to highlight the major issues in calculating the stability boundary in a non-parallel analysis. But to present quantitative results, we need to consider special cases. Consider then, the physical streamwise disturbance velocity given by

$$\tilde{u}_d = \Delta\left\{ D\hat{\phi}\exp\left[i\left(\int_{x_0}^{x}\alpha\,dx - \omega t\right)\right]\right\}_r. \qquad (6.1)$$

Note the difference between the quantity u_d (as in (5.2)-(5.4)) and $\tilde{u}_d$ above, the latter being simply the real-part of the former. In linear stability analysis, the governing equations are linear in the perturbation quantities. Therefore the real and imaginary parts of the equations can be decoupled. Since complex analysis

61

simplifies mathematical treatment, the perturbation waveforms are easier expressed as full-complex quantities.

But the growth rate (see (3.26), (5.24)) of a physical quantity necessitates a non-linear algebraic operation (division of the rate of change of the quantity by the quantity itself). Hence to obtain a physically relevant interpretation of the stability characteristics, care must be taken to consider only the real part of the disturbance field.

6.2 Trajectory

Following (6.1) we consider the rate of change of $\tilde{u}_d$ along a trajectory

$$\xi(x_d, y_d) = 0, \tag{6.2}$$

which is given by

$$\frac{\partial \tilde{u}_d}{\partial s} = \frac{\left(\dfrac{\partial \tilde{u}_d}{\partial x_d} \dfrac{\partial \xi}{\partial y_d} - \dfrac{\partial \tilde{u}_d}{\partial y_d} \dfrac{\partial \xi}{\partial x_d} \right)}{\left[\left(\dfrac{\partial \xi}{\partial x_d} \right)^2 + \left(\dfrac{\partial \xi}{\partial y_d} \right)^2 \right]^{1/2}}, \tag{6.3}$$

where ∂s is an infinitesimal length along ξ. This rate of change can be non-dimensionalized by defining

$$g_u \equiv \frac{\delta_\omega}{\tilde{u}_d} \left(\frac{\partial \tilde{u}_d}{\partial x_d} \frac{\partial \xi}{\partial y_d} - \frac{\partial \tilde{u}_d}{\partial y_d} \frac{\partial \xi}{\partial x_d} \right). \tag{6.4}$$

Now, for example with $\xi = y_d$ (along a straight line parallel to the x_d-axis), we have

$$g_u = \frac{\delta_\omega}{\tilde{u}_d} \frac{\partial \tilde{u}_d}{\partial x_d}, \tag{6.5}$$

and with $\xi = y$ (along a streamline), we have

$$g_u = \frac{1}{\tilde{u}_d} \frac{\partial \tilde{u}_d}{\partial x}, \qquad (6.6)$$

both of these being familiar definitions in non-parallel theory. Equations (6.4)–(6.5) restate the fact that in non-parallel analysis, the growth rate, and consequently the stability boundary, depends on the trajectory.

6.3   Integral definition

Alternative definitions of the growth-rate can be constructed specifically to remove the dependence on the trajectory. Consider the integrals

$$\mathfrak{U}_d \equiv \int_{-\infty}^{\infty} \tilde{u}_d \mathrm{d}y, \qquad (6.7)$$

$$\text{and} \qquad \overline{\mathfrak{U}}_d \equiv \int_{-\infty}^{\infty} \tilde{u}_d \mathrm{d}\left(\frac{y_d \Delta}{\nu}\right). \qquad (6.8)$$

Both integrals are performed over the physical domain y_d, but the first one is scaled by the local vorticity-thickness δ_ω, whereas the second one uses (ν/Δ) as the length-scale which is constant for all streamwise locations. In either case, $\mathfrak{U}_d$ and $\overline{\mathfrak{U}}_d$ are independent of any specific y. The advantage of (6.7), (6.8) is that the net stability behaviour of the flow at a particular cross-section is obtained by considering

$$g_{\mathfrak{U}} \equiv \frac{\delta_\omega}{\mathfrak{U}_d} \frac{\mathrm{d}\mathfrak{U}_d}{\mathrm{d}x_d}, \qquad (6.9)$$

$$\text{or} \qquad g_{\overline{\mathfrak{U}}} \equiv \frac{\delta_\omega}{\overline{\mathfrak{U}}_d} \frac{\mathrm{d}\overline{\mathfrak{U}}_d}{\mathrm{d}x_d}. \qquad (6.10)$$

6.4   Time-averaging

Since all disturbance quantities are waveforms, it is straightforward to deduce that the growth-rate definitions given in the preceding sections will contain a sinusoidal phase component dependent on time. As an example, expanding definition (6.4), we get

$$g_u = r \frac{\cos{(\Psi + \Theta)}}{\cos{(\Xi + \Theta)}},$$
(6.11)

where

$$r = \left| \frac{\partial_x \mathrm{D}\hat{\phi}}{\mathrm{D}\hat{\phi}} + \mathrm{i}\alpha \right|,$$
(6.12)

$$\Theta = \int_{x_0}^{x} \alpha_r \mathrm{d}x - \omega t,$$
(6.13)

$$\Psi = \mathrm{Arg}\left(\partial_x \mathrm{D}\hat{\phi} + \mathrm{i}\alpha \mathrm{D}\hat{\phi} \right)$$
(6.14)

$$\text{and} \quad \Xi = \mathrm{Arg}\left(\mathrm{D}\hat{\phi} \right).$$
(6.15)

(Here Arg is the argument of a complex quantity.) To remove the time-dependence in the growth-rate, we consider, instead of the amplification of the waveform $\tilde{u}_d$, the amplification of its intensity $\tilde{u}_d^2$ averaged over one time-period. The intensity does not average to zero over one time-period, but the waveform $\tilde{u}_d$ would. Hence, we have

$$\langle g_{u^2} \rangle \equiv \frac{1}{\langle \tilde{u}_d^2 \rangle} \frac{\partial \langle \tilde{u}_d^2 \rangle}{\partial x},$$
(6.16)

where

$$\langle \tilde{u}_d^2 \rangle = \left(\frac{\omega_d}{2\pi} \right) \exp\left(-2 \int_{x_0}^{x} \alpha_i \mathrm{d}x \right) J \Delta^2,$$
(6.17)

and

$$J = \int_{t_d}^{t_d + (2\pi/\omega_d)} \left\{ \mathrm{D}\hat{\phi} \exp\left[\mathrm{i} \left(\int_{x_0}^{x} \alpha_r \mathrm{d}x - \omega_d \tau \right) \right] \right\}_r^2 \mathrm{d}\tau.$$

Now, the averaging operation leads to

$$\frac{1}{4}(D\hat{\phi})^2 \exp\left(2i\int_{x_0}^x \alpha_r dx\right) \int_{t_d}^{t_d+(2\pi/\omega_d)} \exp\left(-2i\omega_d\tau\right) d\tau = 0,$$

$$\frac{1}{4}(D\hat{\phi}^*)^2 \exp\left(-2i\int_{x_0}^x \alpha_r dx\right) \int_{t_d}^{t_d+(2\pi/\omega_d)} \exp\left(2i\omega_d\tau\right) d\tau = 0$$

$$\text{and} \quad \frac{1}{2}\left|D\hat{\phi}\right|^2 \int_{t_d}^{t_d+(2\pi/\omega_d)} d\tau = \frac{1}{2}\left|D\hat{\phi}\right|^2 \frac{2\pi}{\omega_d},$$

$$\Rightarrow \langle \tilde{u}_d^2 \rangle = \frac{\Delta^2}{2}\left|D\hat{\phi}\right|^2 \exp\left(-2\int_{x_0}^x \alpha_i dx\right). \tag{6.18}$$

Simplifying (6.16) using (6.18) we get

$$\langle g_{u^2} \rangle = -2\alpha_i + 2\left(\frac{\partial_x D\hat{\phi}}{D\hat{\phi}}\right)_r. \tag{6.19}$$

6.5 Time-averaged integrated kinetic energy

Growth rates of the normal velocity $\tilde{v}_d$, kinetic-energy $k_d \equiv \frac{1}{2}\left(\tilde{u}_d + \tilde{v}_d^2\right)$, vorticity $\Omega_d \equiv \left(\frac{\partial \tilde{u}_d}{\partial y_d} - \frac{\partial \tilde{v}_d}{\partial x_d}\right)$, enstrophy Ω_d^2, etc. of the disturbance field can be defined and equations corresponding to (6.4), (6.9), (6.10) and (6.19) obtained in a similar fashion. To present the stability results in the next chapter, however, the following definition of growth-rate is used:

$$g \equiv \langle g_K \rangle = \frac{1}{\langle K \rangle}\frac{d}{dx}\langle K \rangle, \tag{6.20}$$

where

$$K = \int_{-\infty}^{\infty} k_d \, dy, \tag{6.21}$$

and

$$\tilde{v}_d = -\Delta \left\{ \left(\frac{p}{\mathrm{Re}} + i\alpha + \partial_x - \frac{py}{\mathrm{Re}} \mathrm{D} \right) \hat{\phi} \exp \left[i \left(\int_{x_0}^x \alpha_r \mathrm{d}x - \omega t \right) \right] \right\}_r . \qquad (6.22)$$

(For later use, we also define the quantity $\overline{K}$

$$\overline{K} = \int_{-\infty}^{\infty} k_d \, \mathrm{d} \left(\frac{y_d \Delta}{\nu} \right) , \qquad (6.23)$$

which is the total disturbance kinetic-energy at a given streamwise location.) Using (6.1) and (6.22) in (6.21), and subsequently (5.21) for $\hat{\phi}$, we get

$$g = -2\alpha_i + 2 \left(\frac{1}{A} \frac{\mathrm{d}A}{\mathrm{d}x} \right)_r + 2 \frac{\displaystyle\int_{-\infty}^{\infty} J_1(y) \mathrm{d}y}{\displaystyle\int_{-\infty}^{\infty} J_2(y) \mathrm{d}y} + o(\mathrm{Re}^{-1}), \qquad (6.24)$$

which is the spatial growth-rate correct to $O\left(\mathrm{Re}^{-1}\right)$. Here,

$$J_1(y) = \left(\mathrm{D}\hat{\phi}_m^* \partial_x \mathrm{D}\hat{\phi}_m \right)_r$$
$$+ |\alpha|^2 \left(\hat{\phi}_m^* \partial_x \hat{\phi}_m \right)_r + \left| \hat{\phi}_m \right|^2 (\alpha^* \alpha')_r , \qquad (6.25)$$

$$\mathrm{and} \quad J_2(y) = \left| \mathrm{D}\hat{\phi}_m \right|^2 + \left| \alpha \hat{\phi}_m \right|^2 . \qquad (6.26)$$

Note that the quantity K in (6.21) is not the total disturbance kinetic-energy at a given streamwise location. This is because in the similarity coordinate y depends on the local vorticity-thickness. In fact the quantity $\overline{K}$ is the integral of the total kinetic energy at a given streamwise location. Note that $\langle \overline{K} \rangle \propto \mathrm{Re}\langle K \rangle$, and therefore the streamwise rate of change of $\langle \overline{K} \rangle$ would incorporate the rate of spreading of the mixing layer in addition to the growth-rate given by g above. The rates $\mathrm{d}\langle \overline{K} \rangle / \mathrm{d}x$ and $\mathrm{d}\langle K \rangle / \mathrm{d}x$ can be very different, owing to the fact that

Re depends on x. In this case the interpretation given in Lessen & Ko (1966) that p/Re represents "a rate of disturbance-energy dilution" is found to be misleading.

6.6   Computation method

To each point on the marginal stability boundary, a particular value of $\omega_d \nu / \Delta^2$ is chosen. Then with a guess value of the Reynolds number Re_1 and a particular choice of δRe_1 the eigenvalue problem (5.18) is solved at Re_1 and $\text{Re}_1 + \delta\text{Re}_1$. The eigenfunction $\hat{\phi}_m$ is normalized, unless otherwise specified, using (4.12). The growth-rate $g(\omega_d \nu / \Delta^2, \text{Re})$, given by (6.24), is then obtained by using (5.35), (5.29). A similar procedure is used for α'. Using another guess value for the Reynolds number Re_2 (where $\text{Re}_1, \text{Re}_2 \gg |\text{Re}_2 - \text{Re}_1| \gg \delta\text{Re}_1, \delta\text{Re}_2$) we obtain $g(\omega_d \nu / \Delta^2, \text{Re}_2)$ for the same mode.

A standard Newton–Raphson procedure is now employed to converge to the particular value of Reynolds number Re_s such that $g(\omega_d \nu / \Delta^2, \text{Re}_s) = 0$. For different values of ω_d, the curve of marginal stability can now be traced in the α–Re plane. The eigenvalue problem (5.18) is posed with α as the eigenvalue, the procedure for which is detailed in § 4.3. The matrices $\mathbf{L}_A$ and $\mathbf{L}_B$ of (4.14) are different and can be found detailed in Appendix C.

Apart from the parameters N, L, S and b (see § 3.4, (4.1) and (4.2)) that were required to be specified in solving the Orr–Sommerfeld equation – and the same holds true for the minimal composite equation – the additional parameter δRe is needed for computing the forward-differences. Sufficient accuracy of the difference is obtained if δRe is taken to be 2% of Re. A smaller step-size than this causes the difference between the values dependent on Re to become smaller than their respective accuracy levels, and therefore the value of the derivative becomes

suspect.

To solve the matrix form of the adjoint problem, the *ZGESV* from the **LA-PACK** library is used. The integrals of the kinetic energy and those in (5.35) in the infinite y-domain are computed as follows. The integrand is assumed to decay exponentially in the far-field. Thus the y-domain is taken sufficiently large such that the contribution from the infinite tails $y \in [\pm L, \pm \infty)$, can be computed from an analytic expression. Specifically, if $\rho(y)$ be some complex-valued function, then

$$\int_{-\infty}^{\infty} \rho \, \mathrm{d}y = \int_{-L}^{L} \rho \, \mathrm{d}y - \frac{\rho_L^2}{\mathrm{D}\rho_L} + \frac{\rho_{-L}^2}{\mathrm{D}\rho_{-L}}, \qquad (6.27)$$

where the subscript $\pm L$ denotes the y-location where the quantity is computed. The y-derivative $\mathrm{D}\rho$ can be computed to a high order of accuracy using the spectral collocation derivate-matrix $\mathbf{D}$. For most of the computations it was however found that the domain was already sufficiently large such that the contribution from the tail regions was orders of magnitude ($\approx 10^{-14}$) smaller than that from the finite region under consideration.

CHAPTER 7

NON-PARALLEL STABILITY RESULTS

In this chapter results on the linear stability characteristics of a two-dimensional mixing layer are presented in the context of a spatial analysis. Following the preceding chapter, the streamwise evolution of the quantity K (see 6.21), corresponding to a particular disturbance mode given by a constant dimensional frequency ω_d, is monitored. This reduces the effort of reporting results for different y-locations. The location of switchover from decay to growth along the Re-axis marks the point on the stability boundary corresponding to this frequency. Moving along a continuous range of such frequencies, the curve of marginal stability can be mapped.

Unlike temporal analysis, spatial analysis is not invariant under a Galilean-transformation (that is, with respect to the eigenvalue α). Therefore the computations must be carried out separately for each velocity ratio. Velocity ratios with backflow ($|\Lambda| > 1$) are not considered, the streamwise direction being ambiguous in these situations, as remarked before. However, and surprisingly, for all co-flowing configurations, the velocity and length scales of Δ and δ_ω seem to be quite a judicious choice, the results then being only weakly dependent on Λ.

7.1   Stability results for $\Lambda = 1$ (halfjet)

Of all co-flowing configurations, the $\Lambda = 1$ case would intuitively appear to be the most unstable. This is because it lies at the opposite extreme of the $\Lambda = 0$ (shearless

flow) case. Therefore, we first present the stability results focusing on this case. For other values of Λ, we make comparisons in the section that follows. The curve
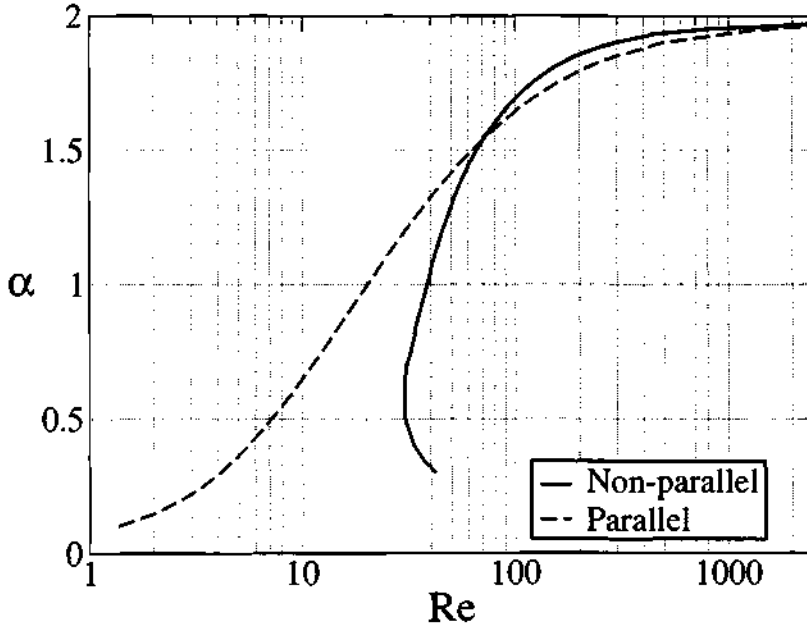
Figure 7.1: Marginal stability curve for the $\Lambda = 1$ (halfjet) case. The stability boundary is based on the growth-rate (6.24).

of marginal stability for the halfjet is presented in figure 7.1. Table 7.1 presents the numerical values at indicative locations along the curve. As mentioned before, we do not present the dependence of results on the parameters of computation, though typical values are mentioned alongside. An exercise identical to that in chapter 4 was carried out to ensure that the results are independent of small changes in the parameters.

Figures 7.2–7.5 present the real and imaginary parts of the eigenfunctions, normalized using (4.12), at some of the points in table 7.1. Recall that it is not meaningful to seek the streamwise-gradient of the minimal eigensolution $\partial\hat{\phi}_m/\partial x$, since it is inevitably based on the choice of normalization. But the dependence of

Re	ω	α_r	α_i	zero
3195.8	1.160	1.973	0.001	10^{-5}
486.8	1.130	1.938	0.000	10^{-5}
283.9	1.100	1.900	−0.003	10^{-5}
205.4	1.070	1.862	−0.008	10^{-5}
163.0	1.040	1.823	−0.015	10^{-5}
135.4	1.010	1.784	−0.022	10^{-5}
116.6	0.980	1.744	−0.030	5×10^{-5}
102.4	0.950	1.704	−0.039	5×10^{-5}
91.4	0.920	1.662	−0.049	5×10^{-5}
84.1	0.890	1.625	−0.058	5×10^{-5}
76.9	0.860	1.582	−0.069	5×10^{-5}
69.7	0.830	1.534	−0.081	5×10^{-5}
65.0	0.800	1.491	−0.092	5×10^{-5}
60.7	0.770	1.446	−0.104	5×10^{-5}
57.1	0.740	1.401	−0.116	5×10^{-5}
53.9	0.710	1.354	−0.128	5×10^{-5}
50.8	0.680	1.306	−0.140	10^{-4}
48.2	0.650	1.260	−0.151	10^{-4}
46.0	0.620	1.213	−0.163	10^{-4}
43.8	0.590	1.163	−0.174	10^{-4}
41.8	0.560	1.109	−0.186	10^{-4}
40.0	0.530	1.054	−0.197	10^{-4}
38.4	0.500	0.998	−0.207	8×10^{-4}
36.7	0.470	0.940	−0.216	8×10^{-4}
35.0	0.440	0.879	−0.223	8×10^{-4}
33.5	0.410	0.817	−0.229	8×10^{-4}
32.2	0.380	0.753	−0.232	8×10^{-4}
30.5	0.350	0.687	−0.232	8×10^{-4}
30.1	0.320	0.619	−0.231	8×10^{-4}
30.1	0.290	0.549	−0.227	8×10^{-4}
30.6	0.260	0.478	−0.218	8×10^{-4}
33.1	0.230	0.406	−0.206	8×10^{-4}
38.6	0.200	0.334	−0.190	8×10^{-4}

Table 7.1: Marginal modes along the stability boundary for $\Lambda = 1$.

stability results on the choice of normalization can be appraised. Consider then an

alternative normalization scheme,

$$\hat{\phi}_m(0) = 1 + i0. \tag{7.1}$$

The stability computations corresponding to (7.1) appear in table 7.2, only indicative values along the curve being presented. Comparing with table 7.1, we note that the dependence of the results on the choice of normalization is negligible throughout the marginal stability curve.

Table 7.3 shows the values of the quantity α' along the stability boundary. The assumption that this quantity scales as $O\left(\text{Re}^{-1}\right)$ seems justified. Note that the real part of the wavenumber α_r determines its order of magnitude and is $O(1)$. The imaginary part of the wavenumber α_i on the other hand contributes to the growth-rate (6.24). From the slowly-varying assumption, all the other terms in that expression, which arise from non-parallel contributions, are $O\left(\text{Re}^{-1}\right)$. Therefore, this assumption would hold if $\alpha_i \sim O\left(\text{Re}^{-1}\right)$ on the curve of marginal stability, where the contributions must balance each other out up to a numerical zero. Table 7.1 shows that this condition is met quite satisfactorily. As mentioned before, the choice of normalization shifts the weight from one part of the non-parallel con-

Re	ω	α_r	α_i	zero
283.9	1.100	1.900	-0.003	10^{-5}
205.3	1.070	1.861	-0.007	10^{-5}
102.4	0.950	1.704	-0.038	10^{-5}
91.4	0.920	1.662	-0.049	5×10^{-5}
50.9	0.680	1.306	-0.140	10^{-4}
32.2	0.380	0.752	-0.233	6×10^{-4}
30.1	0.290	0.549	-0.227	8×10^{-4}
33.1	0.230	0.407	-0.206	8×10^{-4}

Table 7.2: Marginal modes along the stability boundary for $\Lambda = 1$, with normalization scheme (7.1) used instead of (4.12).
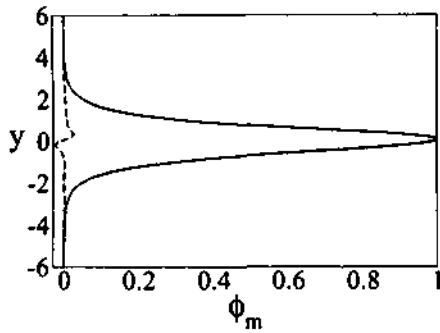
Figure 7.2: $\alpha = 1.862 - 0.008i$, Re = 205.4, $\omega = 1.070$
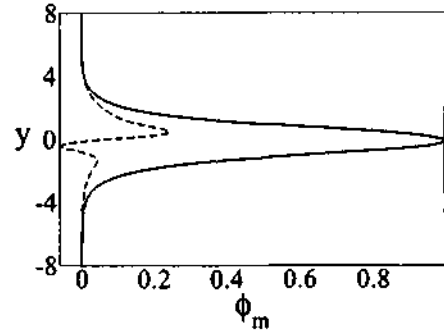
Figure 7.3: $\alpha = 1.306 - 0.140i$, Re = 50.8, $\omega = 0.680$
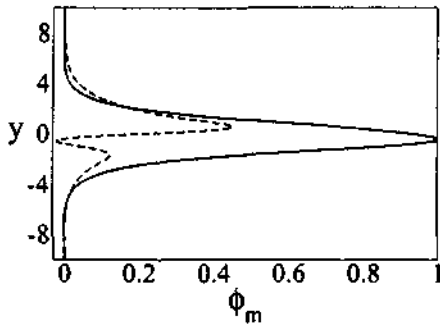
Figure 7.4: $\alpha = 0.940 - 0.216i$, Re = 36.7, $\omega = 0.470$
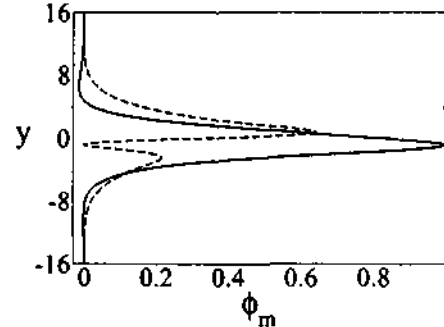
Figure 7.5: $\alpha = 0.549 - 0.227i$, Re = 30.1, $\omega = 0.290$

Eigensolution $\hat{\phi}_m(y)$ to the minimal equation (5.18), corresponding to different points on the marginal stability curve (see figure 7.1).
Solid line, real-part; dashed-line, imaginary-part.

Re	α	$(Re/p)|\alpha'/\alpha|$
205.4	$1.862 - 0.008i$	0.306
50.8	$1.306 - 0.140i$	0.337
36.7	$0.940 - 0.216i$	0.376
30.1	$0.549 - 0.227i$	0.425

Table 7.3: Streamwise-gradient of the wavenumber, for different points on the stability boundary corresponding to $\Lambda = 1$.

tribution to another, the sum nevertheless remaining the same. Thus the effect of $\partial\hat{\phi}_m/\partial x$ and $(1/A)dA/dx$ are invariant when considered cumulatively; the only meaningful way of assessing their effect is by considering the sum $g_{np} = g + 2\alpha_i$.

Thus, we believe that the slowly-varying assumptions

$$\alpha', \frac{\partial \hat{\phi}_m}{\partial x}, \frac{1}{A}\frac{\mathrm{d}A}{\mathrm{d}x} \sim O\left(\mathrm{Re}^{-1}\right), \tag{7.2}$$

separately, are also justified.

Re	α	$\lvert y_c\rvert/(\lvert\alpha\rvert\mathrm{Re})^{-1/3}$
205.4	$1.862 - 0.008i$	0.092
50.8	$1.306 - 0.140i$	0.284
36.7	$0.940 - 0.216i$	0.332
30.1	$0.549 - 0.227i$	0.262

Table 7.4: Distance of the critical point from the inflexion point, normalized by the critical layer thickness, for different points on the stability boundary corresponding to $\Lambda = 1$.

The final assumption that needs to be verified is the proximity of the critical point to the inflexion point of the mean-profile. Table 7.4 presents the quantity $(y_c - y_s) = y_c$ along the stability boundary, normalized by the thickness of the critical-layer $(\lvert\alpha\rvert\mathrm{Re})^{-1/3}$ It is seen that the critical point is sufficiently close to $y = 0$. It hence follows that the expressions (5.14) and (5.15) are valid approximations.

Another a posteriori check of the validity of the large Re approximation, which was also presented in Bhattacharya *et al.* (2006), is obtained as follows. First, a measure of the error in the present analysis, in relation to a solution of the full non-parallel equation (5.9), is constructed. As the primary approximation made here is the neglect of the higher-order operator $\mathcal{H}$, an obvious measure of the error is

$$h \equiv \frac{\langle \mathcal{H}\hat{\phi}_m, \mathcal{H}\hat{\phi}_m\rangle}{\langle \hat{\phi}_m, \hat{\phi}_m\rangle}, \tag{7.3}$$

where $(,)$ denotes the inner product

$$\langle f, g \rangle = \int_{-\infty}^{\infty} fg^* \mathrm{d}y. \tag{7.4}$$

Λ	h	Re_m
1/7	0.0001197	46.8
1/3	0.0002678	48.7
3/5	0.0003067	40.8
1	0.0003969	32.3

Table 7.5: Norm of the $\mathcal{H}$ operator. Re_m is the value of the Reynolds numberat which h takes the maximum value along the marginal stability curve for a given Λ.

The quantity h is related to the norm of the operator $\mathcal{H}$, which is defined here as the smallest number h for which $\|\mathcal{H}\phi_m\| \leq h\|\phi_m\|$ (following Liusternik & Sobolev, 1961, p. 82), evaluating the right-hand side of (7.3) along the marginal stability loop. The values of h for different values of Λ are listed in table 7.5. The highest value, which occurs at $\Lambda = 1$, is of order 4×10^{-4}; it drops to 1×10^{-4} at $\Lambda = 1/7$. This suggests that the error is indeed small, particularly at small Λ.

7.2   Results for other Λ

Marginal stability curves, corresponding to the quantity K, are shown in figures 7.6–7.9 for $\Lambda = 3/5$, 1/3, 1/7 and 1/39. Typical parameters used on the computations are listed alongside frequencies, corresponding to points along the stability boundary, in tables 7.6–7.9.

Tables 7.10–7.13 compare the non-parallel and parallel contributions to the growth-rate. For the sake of brevity, other quantities of relevance are also presented in the same tables. We note that the slowly-varying assumption holds good throughout the range of velocity ratios considered. In fact as the $\Lambda \to 0$ (shearless flow) limit is approached, this approximation becomes increasingly accurate.

7.3 Critical Reynolds number

From figures 7.1,7.6–7.9, the result of paramount importance is that the critical Reynolds number Re_c is found to be about 30 for all Λ. In fact as the limit $\Lambda \to 0$ is approached, this value remains unchanged, and essentially a non-zero finite number. The significance of this result can be seen if one expresses the Reynolds number in the conventional scales of U_∞ and θ. Defining

$$\text{Re}^* \equiv \frac{U_\infty \theta}{\nu} = \text{Re}\frac{\theta}{\delta_\omega}\frac{U_\infty}{\Delta}, \tag{7.5}$$
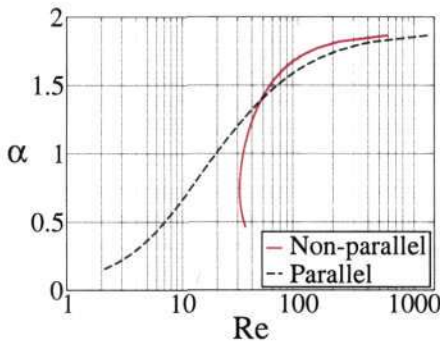
Figure 7.6: $\Lambda = 3/5$
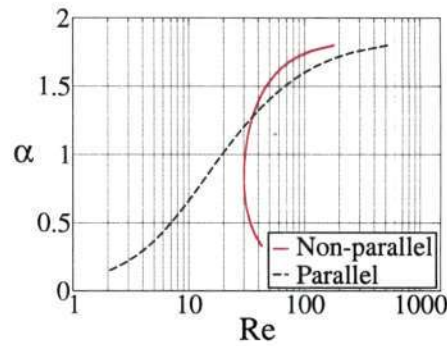
Figure 7.7: $\Lambda = 1/3$
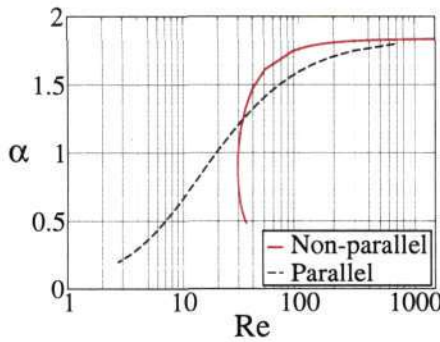
Figure 7.8: $\Lambda = 1/7$
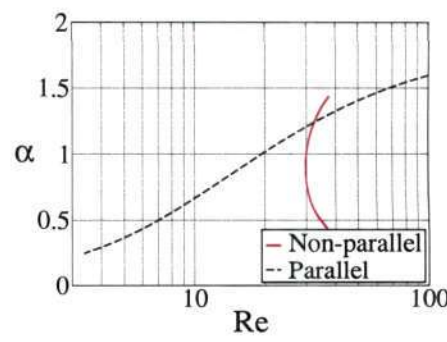
Figure 7.9: $\Lambda = 1/39$

Marginal stability curves for different values of the velocity-ratio parameter Λ.

Re	ω	α_r	α_i	zero
601.5	1.650	1.866	0.002	10^{-5}
225.5	1.600	1.819	0.001	10^{-5}
145.9	1.550	1.771	−0.003	10^{-5}
110.4	1.500	1.723	−0.009	10^{-5}
89.9	1.450	1.673	−0.016	10^{-5}
76.5	1.400	1.623	−0.024	10^{-5}
66.9	1.350	1.573	−0.033	10^{-5}
66.8	1.350	1.573	−0.033	10^{-5}
59.7	1.300	1.521	−0.042	10^{-5}
54.2	1.250	1.469	−0.051	10^{-5}
49.8	1.200	1.416	−0.061	10^{-5}
46.3	1.150	1.363	−0.071	5×10^{-4}
43.3	1.100	1.308	−0.080	5×10^{-4}
40.8	1.050	1.253	−0.089	5×10^{-4}
38.7	1.000	1.197	−0.098	5×10^{-4}
36.9	0.950	1.140	−0.107	5×10^{-4}
35.4	0.900	1.082	−0.115	5×10^{-4}
34.1	0.850	1.023	−0.122	5×10^{-4}
33.2	0.800	0.963	−0.129	5×10^{-4}
32.4	0.750	0.903	−0.134	5×10^{-4}
31.8	0.700	0.841	−0.138	5×10^{-4}
31.5	0.650	0.779	−0.141	5×10^{-4}
31.4	0.600	0.716	−0.143	5×10^{-4}
31.7	0.550	0.652	−0.143	5×10^{-4}
32.3	0.500	0.589	−0.141	5×10^{-4}
33.4	0.450	0.525	−0.137	5×10^{-4}
35.2	0.400	0.461	−0.131	5×10^{-4}

Table 7.6: Marginal modes along the stability boundary for $\Lambda = 3/5$.

and noting that Re_c and δ_ω/θ are finite in the limit $\Lambda \to 0$, we find that

$$\mathrm{Re}_c^*(\Lambda \to 0) \to \infty. \tag{7.6}$$

This result is of immediate appeal as it recovers the intuitive notion that in the absence of mean shear, the flow should be stable at all Reynolds numbers. Moreover, from table 7.14, which records Re_c and Re_c^* for different Λ, it is seen

Re	ω	α_r	α_i	zero
128.6	2.700	1.771	0.006	10^{-5}
84.5	2.600	1.709	0.003	10^{-5}
65.7	2.500	1.647	−0.002	10^{-5}
55.1	2.400	1.584	−0.008	6×10^{-5}
48.2	2.300	1.521	−0.015	6×10^{-5}
43.5	2.200	1.457	−0.022	6×10^{-5}
39.9	2.100	1.394	−0.030	6×10^{-5}
37.3	2.000	1.329	−0.037	6×10^{-5}
35.2	1.900	1.265	−0.044	2×10^{-4}
33.6	1.800	1.199	−0.051	2×10^{-4}
32.3	1.700	1.134	−0.057	2×10^{-4}
31.5	1.600	1.068	−0.063	2×10^{-4}
30.7	1.500	1.001	−0.067	2×10^{-4}
30.2	1.400	0.935	−0.071	2×10^{-4}
30.0	1.300	0.867	−0.075	2×10^{-4}
29.9	1.200	0.800	−0.077	2×10^{-4}
30.2	1.100	0.732	−0.078	2×10^{-4}
30.7	1.000	0.665	−0.078	2×10^{-4}
31.6	0.900	0.597	−0.077	2×10^{-4}
33.1	0.800	0.529	−0.075	2×10^{-4}
35.1	0.700	0.461	−0.072	2×10^{-4}
38.3	0.600	0.393	−0.067	2×10^{-4}
43.1	0.500	0.325	−0.060	2×10^{-4}

Table 7.7: Marginal modes along the stability boundary for $\Lambda = 1/3$.

that the halfjet case becomes unstable at the lowest Reynolds number, the onset of instability getting progressively delayed with the mean-shear getting smaller. The corresponding critical modes identified by α_c, ω_c for the values of Λ considered appear in the same table. Further, that the critical Reynolds number found from the present stability calculations is as high as 30 lends support to the applicability of the underlying assumptions: the use of the similarity solution for the mean flow and modal approach to describe stability characteristics.

Re	ω	α_r	α_i	zero
1713.1	6.450	1.838	0.001	10^{-5}
448.5	6.420	1.830	0.002	10^{-5}
285.6	6.390	1.821	0.003	10^{-5}
208.5	6.360	1.813	0.004	10^{-5}
170.5	6.330	1.804	0.005	10^{-5}
146.7	6.300	1.796	0.005	10^{-5}
129.0	6.270	1.787	0.005	10^{-5}
116.4	6.240	1.779	0.005	10^{-5}
106.3	6.210	1.770	0.006	10^{-5}
98.8	6.180	1.762	0.006	10^{-5}
92.4	6.150	1.753	0.005	10^{-5}
90.5	6.150	1.753	0.006	10^{-5}
51.1	5.650	1.612	0.001	2×10^{-4}
39.8	5.150	1.471	-0.007	2×10^{-4}
34.7	4.650	1.329	-0.015	2×10^{-4}
31.7	4.150	1.187	-0.022	2×10^{-4}
30.4	3.650	1.044	-0.027	2×10^{-4}
30.1	3.500	1.001	-0.029	2×10^{-4}
29.8	3.450	0.987	-0.029	2×10^{-4}
29.8	3.250	0.930	-0.031	2×10^{-4}
29.9	2.800	0.801	-0.033	2×10^{-4}
30.4	2.500	0.715	-0.034	2×10^{-4}
31.1	2.300	0.657	-0.034	2×10^{-4}
31.4	2.200	0.629	-0.034	2×10^{-4}
32.0	2.100	0.600	-0.033	2×10^{-4}
32.4	2.000	0.571	-0.033	2×10^{-4}
33.3	1.900	0.543	-0.033	2×10^{-4}
34.0	1.800	0.514	-0.032	2×10^{-4}
35.3	1.700	0.485	-0.031	2×10^{-4}

Table 7.8: Marginal modes along the stability boundary for $\Lambda = 1/7$.

7.4 Conclusion

We have shown that minimal composite theory demonstrates the existence of a finite non-zero critical Reynolds number and so is able to reconcile linear stability theory with the energy theories of Lin (1955), Lorentz (1907) and Joseph (1966). This a definite step forward from parallel theory, and provides one instance where

Re	ω	α_r	α_i	zero
37.5	28.000	1.436	−0.002	10^{-4}
36.7	27.600	1.415	−0.002	10^{-4}
35.5	26.800	1.374	−0.002	10^{-4}
34.4	26.000	1.333	−0.003	10^{-4}
33.4	25.200	1.292	−0.003	10^{-4}
32.7	24.400	1.251	−0.003	10^{-4}
32.0	23.600	1.210	−0.004	10^{-4}
31.4	22.800	1.169	−0.004	10^{-4}
31.0	22.000	1.128	−0.004	10^{-4}
30.6	21.200	1.087	−0.005	10^{-4}
30.3	20.400	1.046	−0.005	10^{-4}
30.0	19.600	1.005	−0.005	10^{-4}
29.9	18.800	0.964	−0.005	10^{-4}
29.8	18.000	0.923	−0.006	10^{-4}
29.7	17.200	0.882	−0.006	10^{-4}
29.8	16.400	0.841	−0.006	10^{-4}
29.9	15.600	0.800	−0.006	10^{-4}
30.1	14.800	0.759	−0.006	10^{-4}
30.5	14.000	0.718	−0.006	10^{-4}
30.9	13.200	0.677	−0.006	10^{-4}
31.4	12.400	0.636	−0.006	10^{-4}
32.1	11.600	0.595	−0.006	10^{-4}
33.0	10.800	0.554	−0.006	10^{-4}
34.1	10.000	0.513	−0.006	10^{-4}
35.5	9.200	0.472	−0.006	10^{-4}
37.0	8.400	0.431	−0.005	10^{-4}

Table 7.9: Marginal modes along the stability boundary for $\Lambda = 1/39$.

Re	α	$|y_c|/(|\alpha|\mathrm{Re})^{-1/3}$	$(\mathrm{Re}/p)|\alpha'/\alpha|$
225.5	$1.819 + 0.001i$	0.054	0.856
66.9	$1.573 − 0.033i$	0.135	0.888
35.4	$1.082 − 0.115i$	0.202	0.967
31.4	$0.716 − 0.143i$	0.186	1.024

Table 7.10: Quantities of relevance in non-parallel analysis, for different points on the stability boundary corresponding to $\Lambda = 3/5$.

inclusion of flow non-parallelism gives us a qualitatively different result about the stability.

Re	α	$|y_c|/(|\alpha|\mathrm{Re})^{-1/3}$	$(\mathrm{Re}/p)|\alpha'/\alpha|$
128.6	$1.771 + 0.006i$	0.034	0.941
43.5	$1.457 - 0.022i$	0.081	0.965
30.2	$0.935 - 0.071i$	0.101	0.998
38.3	$0.393 - 0.067i$	0.062	1.013

Table 7.11: Quantities of relevance in non-parallel analysis, for different points on the stability boundary corresponding to $\Lambda = 1/3$.

Re	α	$|y_c|/(|\alpha|\mathrm{Re})^{-1/3}$	$(\mathrm{Re}/p)|\alpha'/\alpha|$
285.6	$1.821 + 0.003i$	0.033	0.986
51.1	$1.612 + 0.000i$	0.039	0.990
29.8	$0.930 - 0.031i$	0.058	1.000
33.3	$0.543 - 0.033i$	0.045	1.003

Table 7.12: Quantities of relevance in non-parallel analysis, for different points on the stability boundary corresponding to $\Lambda = 1/7$.

Re	α	$|y_c|/(|\alpha|\mathrm{Re})^{-1/3}$	$(\mathrm{Re}/p)|\alpha'/\alpha|$
34.4	$1.333 - 0.003i$	0.007	1.000
29.9	$0.964 - 0.005i$	0.008	1.000
34.1	$0.513 - 0.006i$	0.007	1.000

Table 7.13: Quantities of relevance in non-parallel analysis, for different points on the stability boundary corresponding to $\Lambda = 1/39$.

Further work is necessary to elucidate the precise physical mechanisms underlying the stabilizing influence of non-parallelism on the mixing layer.

Δ	0.050	0.250	0.500	0.750	1.000
Re_c	29.7	29.8	29.9	31.4	30.1
Re_c^*	165.5	31.5	14.6	9.3	6.0
$(\alpha_c)_r$	0.882	0.987	0.800	0.716	0.549
$(\alpha_c)_i$	-0.006	-0.029	-0.077	-0.143	-0.227
ω_c	17.2	3.45	1.200	0.600	0.290

Table 7.14: The critical Reynolds numbers for different velocity ratios. The corresponding critical mode is identified by α_c, ω_c.

A Order of magnitude analysis in detail

Order of terms appearing in $\mathcal{N}$ are tabulated below. The second column corresponds to the outer region and the third column corresponds to the critical layer. The rightmost column follows from (5.17).

	$y \sim O(1)$	$y \sim O(\delta_c)$	$\delta_c \sim O(\alpha Re)^{-1/3}$
$(\mathbb{U} - c)$	1	δ_c	$(\alpha Re)^{-1/3}$
$\mathbb{F}$	1	δ_c	$(\alpha Re)^{-1/3}$
$\mathbb{D}^k$	1	δ_c^{-k}	$(\alpha Re)^{k/3}$
∂_x	Re^{-1}	Re^{-1}	Re^{-1}
α'	αRe^{-1}	αRe^{-1}	αRe^{-1}
$(\mathbb{U} - c)\,\mathbb{D}^2$	1	δ_c^{-1}	$(\alpha Re)^{1/3}$
$(\mathbb{U} - c)\,\alpha^2$	α^2	$\alpha^2 \delta_c$	$\alpha^{5/3} Re^{-1/3}$
$\frac{\Phi'''}{2}$	1	δ_c	$(\alpha Re)^{-1/3}$
$-\frac{1}{i\alpha Re}\mathbb{D}^4$	$(\alpha Re)^{-1}$	$(\alpha Re)^{-1}\delta_c^{-4}$	$(\alpha Re)^{1/3}$
$-\frac{1}{i\alpha Re}\alpha^4$	$\alpha^3 Re^{-1}$	$\alpha^3 Re^{-1}$	$\alpha^3 Re^{-1}$
$-\frac{1}{i\alpha Re}2\alpha^2\mathbb{D}^2$	αRe^{-1}	$\alpha Re^{-1}\delta_c^{-2}$	$\alpha^{5/3} Re^{-1/3}$
$-\frac{1}{i\alpha Re}\mathbb{F}\mathbb{D}^3$	$(\alpha Re)^{-1}$	$(\alpha Re)^{-1}\delta_c^{-2}$	$(\alpha Re)^{-1/3}$
$-\frac{1}{i\alpha Re}\mathbb{U}\mathbb{D}^2$	$(\alpha Re)^{-1}$	$(\alpha Re)^{-1}\delta_c^{-2}$	$(\alpha Re)^{-1/3}$

	$y \sim O(1)$	$y \sim O(\delta_c)$	$\delta_c \sim O(\alpha\text{Re})^{-1/3}$
$-\frac{1}{i\alpha\text{Re}}\frac{\Phi''}{2}D$	αRe^{-1}	$\alpha\text{Re}^{-1}\delta_c^{-1}$	$\alpha^{5/3}\text{Re}^{-2/3}$
$-\frac{1}{i\alpha\text{Re}}\alpha^2 c$	αRe^{-1}	αRe^{-1}	αRe^{-1}
$-\frac{1}{i\alpha\text{Re}}\Phi'''$	αRe^{-1}	$(\alpha\text{Re})^{-1}\delta_c$	$(\alpha\text{Re})^{-4/3}$
$-\frac{\alpha^2 y(\mathbb{U}-c)}{i\alpha\text{Re}}D$	αRe^{-1}	$\alpha\text{Re}^{-1}\delta_c$	$\alpha^{2/3}\text{Re}^{-4/3}$
$-\frac{\alpha^2\mathbb{F}}{i\alpha\text{Re}}D$	αRe^{-1}	αRe^{-1}	$\alpha\text{Re}^{-1/3}$
$(3\mathbb{U}-c)\alpha'$	αRe^{-1}	$\alpha\text{Re}^{-1}\delta_c^{-2}$	$\alpha^{5/3}\text{Re}^{-1/3}$
$\frac{1}{i\alpha}\frac{\Phi'''}{2}\partial_x$	$(\alpha\text{Re})^{-1}$	$(\alpha\text{Re})^{-1}\delta_c$	$(\alpha\text{Re})^{-4/3}$
$2\alpha(\mathbb{U}-c)\partial_x$	αRe^{-1}	$\alpha\text{Re}^{-1}\delta_c$	$\alpha^{2/3}\text{Re}^{-4/3}$
$\alpha\mathbb{F}\partial_x$	αRe^{-1}	αRe^{-1}	αRe^{-1}
$\frac{1}{\alpha}\mathbb{U}D^2\partial_x$	$(\alpha\text{Re})^{-1}$	$(\alpha\text{Re})^{-1}\delta_c^2$	$(\alpha\text{Re})^{-1/3}$
$-\frac{1}{i\alpha}\mathcal{S}\partial_x$	$(\alpha\text{Re})^{-1}$	$(\alpha\text{Re})^{-1}\delta_c^2$	$(\alpha\text{Re})^{-1/3}$

Here, for the sake of brevity, the two symbols $\mathbb{U} = \left(\frac{1}{2\Lambda} + \frac{\Phi'}{2}\right)$ and $\mathbb{F} = \left(\frac{y}{2\Lambda} + \frac{\Phi}{2}\right)$ have been introduced. Note that $\alpha \sim O(1)$ in the present analysis. The lowest order terms in each region have been highlighted in red. Further, though $(\Phi'''/2) \sim O(\alpha\text{Re})^{-2/3}$ compared to the lowest order term in the critical region $(y \sim O(\delta_c))$, it has a *numerical* factor Φ_c'''' multiplying it. It has been noted earlier that Φ is comparable to $\tanh 2y$ for the mixing layer. Now $D^4(\tanh 2y) = -16$ at $y = 0$. Therefore the term $(\Phi'''/2)$ is deemed large enough to be retained in the minimal operator even in the critical region. This highlights the fact that the minimal operator is highly dependent on the mean flow in question. Care must be taken to

84

ensure that $\mathcal{M}$ is composed correctly to the distinguished limits in each layer.

B Derivative matrix in spectral collocation

Following Srinivasan *et al.* (1994), the derivative $g' \equiv dg/dy_f$ of a function $g(y_f)$ at the point y_{f_k} (given by the cosine-distribution (4.2)) is

$$g'_k = \sum_{j=1}^{N} d_{kj} g_j, \tag{7}$$

where $g'_j = g'(y_{f_j})$, $g_j = g(y_{f_j})$. Thus the matrix $\mathbf{D}$ can be formed with the element in the k-th row and j-th column d_{kj} being given by

$$
\begin{aligned}
d_{kj} &= \frac{\bar{c}_k}{\bar{c}_j} \frac{(-1)^{k+j}}{(y_{f_k} - y_{f_j})} & 1 \leq k, j \leq N, \quad k \neq j \\
d_{kk} &= -\frac{y_{f_k}}{2(1 - y_{f_k}^2)} & 2 \leq k \leq N - 1, \\
\text{and} \quad d_{11} &= -d_{NN} = \frac{2(N-1)^2 + 1}{6}.
\end{aligned}
\tag{8}
$$

Here, $\bar{c}_1 = \bar{c}_N = 2$ and $\bar{c}_j = 1$ for $2 \leq j \leq N - 1$. Now if $G = \{g_1, g_2, \ldots, g_N\}^{\mathrm{T}}$ and $G' = \{g'_1, g'_2, \ldots, g'_N\}^{\mathrm{T}}$, then

$$G' = \mathbf{D}\, G, \tag{9}$$

where the superscript T denotes the transpose of the vector.

C Minimal operator matrix in spatial analysis

Defining $\varphi_m \equiv [\hat{\phi}_m \quad \alpha \hat{\phi}_m \quad \alpha^2 \hat{\phi}_m]^{\mathrm{T}}$, equation (5.18) can be written as an eigenvalue problem in α as

$$\mathbf{L}_A \varphi_m = \alpha \mathbf{L}_B \varphi_m, \tag{10}$$

85

where

$$\mathbf{L}_A \equiv \begin{bmatrix} 0 & \mathbf{I} & 0 \\ 0 & 0 & \mathbf{I} \\ \mathbf{A}_0 & \mathbf{A}_1 & \mathbf{A}_2 \end{bmatrix}, \tag{11}$$

$$\mathbf{A}_0 = -\omega(\mathbf{FD})^2 - (1/i\mathrm{Re})(\mathbf{FD})^4, \tag{12}$$

$$\mathbf{A}_1 = (1/2)\mathbf{P}_1(\mathbf{FD})^2 + (1/2\Lambda)(\mathbf{FD})^2 - (1/2)\mathbf{P}_3 \tag{13}$$

$$\mathbf{A}_2 = \omega\mathbf{I}, \tag{14}$$

$$\mathbf{L}_B \equiv \begin{bmatrix} \mathbf{I} & 0 & 0 \\ 0 & \mathbf{I} & 0 \\ 0 & 0 & \mathbf{B}_2 \end{bmatrix}, \tag{15}$$

$$\mathbf{B}_2 = (1/2)\mathbf{P}_1 + (1/2\Lambda)\mathbf{I}. \tag{16}$$

References

BALSA, T. F. 1987 On the spatial instability of piecewise linear free shear layers. *J. Fluid Mech.* **174**, 553–563.

BETCHOV, R. & SZEWCZYK, A. 1963 Stability of a shear layer between parallel streams. *Phys. Fluids* **6** (10), 1391–1396.

BHATTACHARYA, P., MANOHARAN, M. P., GOVINDARAJAN, R. & NARASIMHA, R. 2006 The critical Reynolds number of a laminar incompressible mixing layer from minimal composite theory. *J. Fluid. Mech.* **565**, 105–114.

BOUTHIER, M. 1972 Stabilite lineaire des ecoulements presque paralleles. Part I. *J. Méc.* **11**, 599–621.

BOUTHIER, M. 1973 Stabilite lineaire des ecoulements presque paralleles. Part II, La couche limite de Blasius. *J. Méc.* **12**, 75–95.

BRIDGES, T. J. & MORRIS, P. J. 1984 Differential eigenvalue problems in which the parameter appears nonlinearly. *J. Comput. Phys.* **55**, 437–460.

BUN, Y. & CRIMINALE, W. O. 1994 Early period dynamics of an incompressible mixing layer. *J. Fluid Mech.* **273**, 31–82.

CHOMAZ, J.-M. 2005 Global instabilities in spatially developing flows: Non-normality and non-linearity. *Annu. Rev. Fluid Mech.* **37**, 357–392.

CORCOS, G. M. & LIN, S. J. 1984 The mixing layer: deterministic models of a turbulent flow. Part 2. The origin of the three-dimensional motion. *J. Fluid Mech.* **139**, 67–95.

CORCOS, G. M. & SHERMAN, F. S. 1976 Vorticity concentration and the dynamics of unstable free shear layers. *J. Fluid Mech.* **73**, 241–264.

CORCOS, G. M. & SHERMAN, F. S. 1984 The mixing layer: deterministic models of a turbulent flow. Part 1. Introduction and the two-dimensional flow. *J. Fluid Mech.* **139**, 29–65.

COWLEY, S. J. & WU, X.-S. 1994 *Asymptotic approaches to transition modelling*, chap. 3, pp. 1–38. AGARD Rep. 793.

CRAIK, A. D. D. 1980 Nonlinear evolution and breakdown in unstable boundary-layers. *J. Fluid Mech.* **99**, 247–265.

DRAZIN, P. G. & REID, W. H. 2004 In *Hydrodynamic Stability*, 2nd edn. Cambridge University Press.

ESCH, R. 1957 The instability of a shear layer between two parallel streams. *J. Fluid Mech.* **3**, 289–303.

FASEL, H. & KONZELMANN, U. 1990 Non-parallel stability of a flat plate boundary layer using the complete navier-stokes equations. *J. Fluid Mech.* **221**, 311–347.

GASTER, M. 1962 A note on the relation between temporally-increasing and spatially-increasing disturbances in hydrodynamic stability. *J. Fluid Mech.* **14**, 222–224.

GASTER, M. 1974 On the effects of boundary-layer growth on flow stability. *J. Fluid Mech.* **66**, 465–480.

GOVINDARAJAN, R. & NARASIMHA, R. 1995 Stability of spatially developing boundary layers in pressure gradients. *J. Fluid Mech.* **300**, 117–147.

GOVINDARAJAN, R. & NARASIMHA, R. 1997 A low-order theory for stability of non-parallel boundary layer flows. *Proc. R. Soc. Lond.* A **453**, 2537–2549.

GOVINDARAJAN, R. & NARASIMHA, R. 2001 Estimating amplitude ratios in boundary layer stability theory: a comparison between two approaches. *J. Fluid Mech.* **439**, 403–412.

GOVINDARAJAN, R. & NARASIMHA, R. 2005 Accurate estimate of disturbance amplitude variation from solution of minimal composite stability theory. *Theor. Comput. Fluid Dyn.* **19** (4), 229–235.

GROSCH, C. E. & JACKSON, T. L. 1991 Inviscid spatial stability of a three-dimensional compressible mixing layer. *J. Fluid Mech.* **231**, 35–50.

GROSCH, C. E. & SALWEN, H. 1978 The continuous spectrum of the Orr-Sommerfeld equation. Part 1. The spectrum and the eigenfunctions. *J. Fluid Mech.* **87**, 33–54.

GUSTAVSSON, L. H. 1979 Initial-value problem for boundary layer flows. *Phys. Fluids* **22** (9), 1602–1605.

HERBERT, T. 1997 Parabolized stability equations. *Annu. Rev. Fluid Mech.* **29**, 245–283.

HOWARD, L. N. 1961 Note on a paper of John W. Miles. *J. Fluid Mech.* **10**, 509–512.

HUERRE, P. & MONKEWITZ, P. A. 1985 Absolute and convective instabilities in free shear layers. *J. Fluid Mech.* **159**, 151–168.

HUERRE, P. & MONKEWITZ, P. A. 1990 Local and global instabilities in spatially developing flows. *Annu. Rev. Fluid Mech.* **22**, 473–537.

JACKSON, T. L. & GROSCH, C. E. 1991 Inviscid spatial stability of a compressible mixing layer. Part 3. Effect of thermodynamics. *J. Fluid Mech.* **224**, 159–175.

JOSEPH, D. D. 1966 Nonlinear stability of the boussinesq equations by the method of energy. *Archive for Rational Mechanics and Analysis* **22** (3), 163–184.

KO, S.-H. & LESSEN, M. 1969 Low Reynolds number instability of an incompressible half-jet. *Phys. Fluids* **12** (2), 404–407.

KUNDU, P. K. & COHEN, I. M. 2005 *Fluid mechanics*, 3rd edn. Academic Press.

LESSEN, M. & KO, S.-H. 1966 Viscous instability of an incompressible fluid half-jet flow. *Phys. Fluids* **9** (6), 1179–1183.

LIN, C. C. 1955 In *The Theory of Hydrodynamic Stability*. Cambridge University Press.

LINGWOOD, R. J. 1995 Absolute instability of the boundary layer on a rotating disk. *J. Fluid Mech.* **299**, 17–33.

LIUSTERNIK, L. A. & SOBOLEV, V. J. 1961 In *Elements of Functional Analysis*. Constable & Co., London.

LOCK, R. C. 1951 The velocity distribution in the laminar boundary layer between parallel streams. *Q. J. Mech. Appl. Math.* **4** (1), 42–63.

LORENTZ, H. A. 1907 Über die Entstehung turbulenter Flüssigkeitsbewegungen und über den Einfluss dieser Bewegungen bei der Strömung durch Rohren. In *Abhandlungen über Theoret. Physik*. Leipzig.

MARMOTTANT, P. & VILLERMAUX, E. 2004 On spray formation. *J. Fluid Mech.* **498**, 73–111.

METCALFE, R. W., ORSZAG, S. A., BRACHET, M. E., MENON, S. & RILEY, J. J. 1987 Secondary instability of a temporally growing mixing layer. *J. Fluid Mech.* **184**, 207–243.

MICHALKE, A. 1965 On spatially growing disturbances in an inviscid shear layer. *J. Fluid Mech.* **23**, 521.

MONKEWITZ, P. A. & HUERRE, P. 1982 Influence of the velocity ratio on the spatial stability of mixing layers. *Phys. Fluids* **25** (7), 1137–1143.

NARASIMHA, R. & GOVINDARAJAN, R. 2000 Minimal composite equations and the stability of non-parallel flows. *Curr. Sci.* **79** (6), 730–740.

ORR, W. M. F. 1907 The stability or instability of the steady motions of a perfect liquid and of a viscous liquid. Part I: A perfect liquid. Part II: A viscous liquid. *Proc. Roy. Irish Acad.* A **27**, 9–138.

SARIC, W. S. & NAYFEH, A. H. 1975 Non-parallel stability of boundary layer flows. *Phys. Fluids* **18** (8), 945–950.

SCHLICHTING, H. & GERSTEN, K. 2004 *Boundary Layer Theory*, 8th edn. Springer.

SCHMID, P. J. & HENNINGSON, D. S. 2001 *Stability and transition in shear flows*. Springer-Verlag New York, Inc.

SOLOMON, T. H., HOLLOWAY, W. J. & SWINNEY, H. L. 1993 Shear flow instabilities and Rossby waves in barotropic flow in a rotating annulus. *Phys. Fluids* A **5** (8), 1971–1982.

SOMMERFELD, A. 1908 Ein Beitrag zur hydrodynamischen Erklärung der turbulenten Flüssigkeitbewegungen. In *Atti. del 4. Congr. Internat. dei Mat. III*, pp. 116–124. Roma.

SQUIRE, H. B. 1933 On the stability for three-dimensional disturbances of viscous fluid flow between parallel walls. *Proc. Roy. Soc. Lond.* A **142** (847), 621–628.

SRINIVASAN, S., KLIKA, M., LUDWIG, M. H. & RAM, V. V. 1994 A beginner's guide to the use of the spectral collocation method for solving some eigenvalue problems in fluid mechanics. *Tech. Rep.*. National Aerospace Laboratories (Experimental Aerodynamics Division), Bangalore, India.

STEGNER, A., PICHON, T. & BEUNIER, M. 2005 Elliptical-inertial instability of rotating karman vortex streets. *Phys. Fluids* **17**, 066602.

TATSUMI, T. & GOTOH, K. 1960 The stability of free boundary layers between two uniform streams. *J. Fluid Mech.* **7**, 433–441.

TATSUMI, T. & KAKUTANI, T. 1958 The stability of a two-dimensional laminar jet. *J. Fluid Mech* **4**, 261–275.

TING, L. 1959 On the mixing of two parallel streams. *J. Math. and Phys.* **38**, 153–165.

TOLLMIEN, W. 1935 Ein allgemeines Kriterium der Instabilität laminarer Geschwindigkeitsverteilungen. *Nachr. Wiss. Fachgruppe, Göttingen, Math.-phys. Kl.* **1**, 79–114.

VILLERMAUX, E. & REHAB, H. 2000 Mixing in coaxial jets. *J. Fluid Mech.* **425**, 161–185.

VON KARMAN, T. 1921 Über laminare und turbulente Reibung. *Z. Angew. Math. Mech.* **1**, 233–252.

YUAN, L. L., STREET, R. L. & FERZIGER, J. H. 1999 Large-eddy simulations of a round jet in crossflow. *J. Fluid Mech.* **379**, 71–104.